NREL/TP-451-5746 • UC Category: 273 • DE94000250

# High-Efficiency, Thin-Film Solar Cells

## Annual Subcontract Report 1 July 1991 – 30 June 1992

Ronald P. Gale
*Kopin Corporation*
*Taunton, Massachusetts*

NREL technical monitor: J. Benner

National Renewable Energy Laboratory
1617 Cole Boulevard
Golden, Colorado 80401-3393
Operated by Midwest Research Institute
for the U.S. Department of Energy
under Contract No. DE-AC02-83CH10093

Prepared under Subcontract No. XM-0-19142-4

January 1994

## NOTICE



Printed in the United States of America
Available from:
National Technical Information Service
U.S. Department of Commerce
5285 Port Royal Road
Springfield, VA 22161

Price: Microfiche A01
Printed Copy A03

Codes are used for pricing all publications. The code is determined by the number of pages in the publication. Information pertaining to the pricing codes can be found in the current issue of the following publications which are generally available in most libraries: *Energy Research Abstracts (ERA); Government Reports Announcements and Index (GRA and I); Scientific and Technical Abstract Reports (STAR)*; and publication NTIS-PR-360 available from NTIS at the above address.

Printed on recycled paper

# 1. SUMMARY

## 1.1 Objectives

The objectives of this three-year research program are to investigate thin-film GaAs/GaInP cells using the CLEFT technique and to determine the process to enable overgrowth of GaAs films using organometallic chemistry. In the second year, significant advances were made in both of these areas.

## 1.2 GaInP Growth and Characterization

The application of the CLEFT thin-film technique to GaInP/GaAs solar cells and organometallic overgrowth was investigated. Growth experiments were carried out using tertiarybutylphosphine (TBP) as the group 5 source, resulting in GaInP layers grown latticed matched to GaAs. The layers had good surface morphology and exhibited strong room-temperature photoluminescence (PL). A problem of alloy contamination was identified and controlled, leading to higher quality layers.

## 1.3 GaInP Cell Performance

Solar cell structures have been grown and fabricated using the growth parameters for GaAs and GaInP previously determined. With the improved materials developed, significant improvements were made in the performance of the solar cells. Homojunction cells with GaInP window and BSF were fabricated, resulting in series-resistance limited cell efficiencies above 19% AM1.5. Other structures were also investigated.

## 1.4 Organometallic Overgrowth

Conditions for the in situ overgrowth by OMCVD were determined and continuous GaAs layers were grown over a separation mask layer. To enhance the overgrowth ratio and inhibit heterogeneous nucleation, HCl was added to the reactor during growth. The layers were successfully separated from their substrate using the CLEFT process, demonstrating the application of overgrowth using OM chemistry with HCl.

## 2. GaInP GROWTH AND CHARACTERIZATION

We deposited baseline GaInP layers in our research reactor #6. These layers exhibited less than 100 arc-sec of mismatch to GaAs substrates, with a full width at half maximum (FWHM) of 80 arc-sec as measured by double-crystal X-ray diffraction. The layers were In-rich. The surfaces were specular. The room-temperature PL intensity achieved was 3200 mV/mW @654 nm. N-type samples measured by transient PL at NREL showed 6 ns bulk lifetime for 5E17 $cm^{-3}$ Si doping.

Growth conditions developed for the best surface and most narrow X-ray FWHM were at 680°C and 40 torr pressure. The In:Ga ratio was 2.36, and the V:III ratio was 36 using TBP. These conditions resulted in a growth rate of 4.4 um/hr.

### 2.1 SIMS Analysis

These conditions did not guarantee quality material, however. We were growing layers with very low minority-carrier lifetimes, causing poor solar cell performance. Samples of GaInP, GaAs, and GaInAs were grown and sent to NREL's SIMS facility for characterization. The analysis performed by S. Asher of NREL indicated excess indium at the GaInP/GaAs interface. The problem was traced to desorption of material from the reactor walls. A complete clean of the reactor improved the growth, as did changing the indium source. It is not clear that the desorption, or memory, effect was due to an impurity in the indium source or some intermediate compound formation. In addition, pressure was counterbalanced in the manifold to reduce potential composition fluctuations upon flow injection.

The SIMS experiment utilized layers grown from two different OMCVD reactors, with variations introduced in growth temperature, thickness, V/III ratio, and alloy structure. The resulting layers exhibited variations in surface quality and electrical purity. The SIMS analysis included both mass spectra and depth profiles, with both oxygen and cesium beams.

Indium was found in all of the GaAs layers deposited in Reactor #6, while absent from those layers deposited in Reactor #5. Since the latter reactor is only used for the growth of GaAs and AlGaAs, this was confirmation of indium contamination in #6. No other impurities were observed in the bulk of the layers. Phosphorus, which had been unexpectedly seen in GaAs layers grown at the beginning of the program, was absent in all of the GaAs layers, even those capping the GaInP layers. However, the GaInP layers did show an arsenic "tail", evidence of a non-abrupt junction.

### 2.2 Indium Contamination

The indium contamination was evident in GaAs layers grown on GaAs substrates without the indium source opened. Figure 2.1 shows the depth profile of such a layer, with the surface to the left and the substrate to the right. The layer-substrate interface was reached after about 75 minutes of sputtering, and shows background indium (800 counts/sec) in the substrate. With the start of layer growth, the indium signal climbs to 500K counts per second, and slowly decreases to under 20K when the layer thickness of 2.9 um is

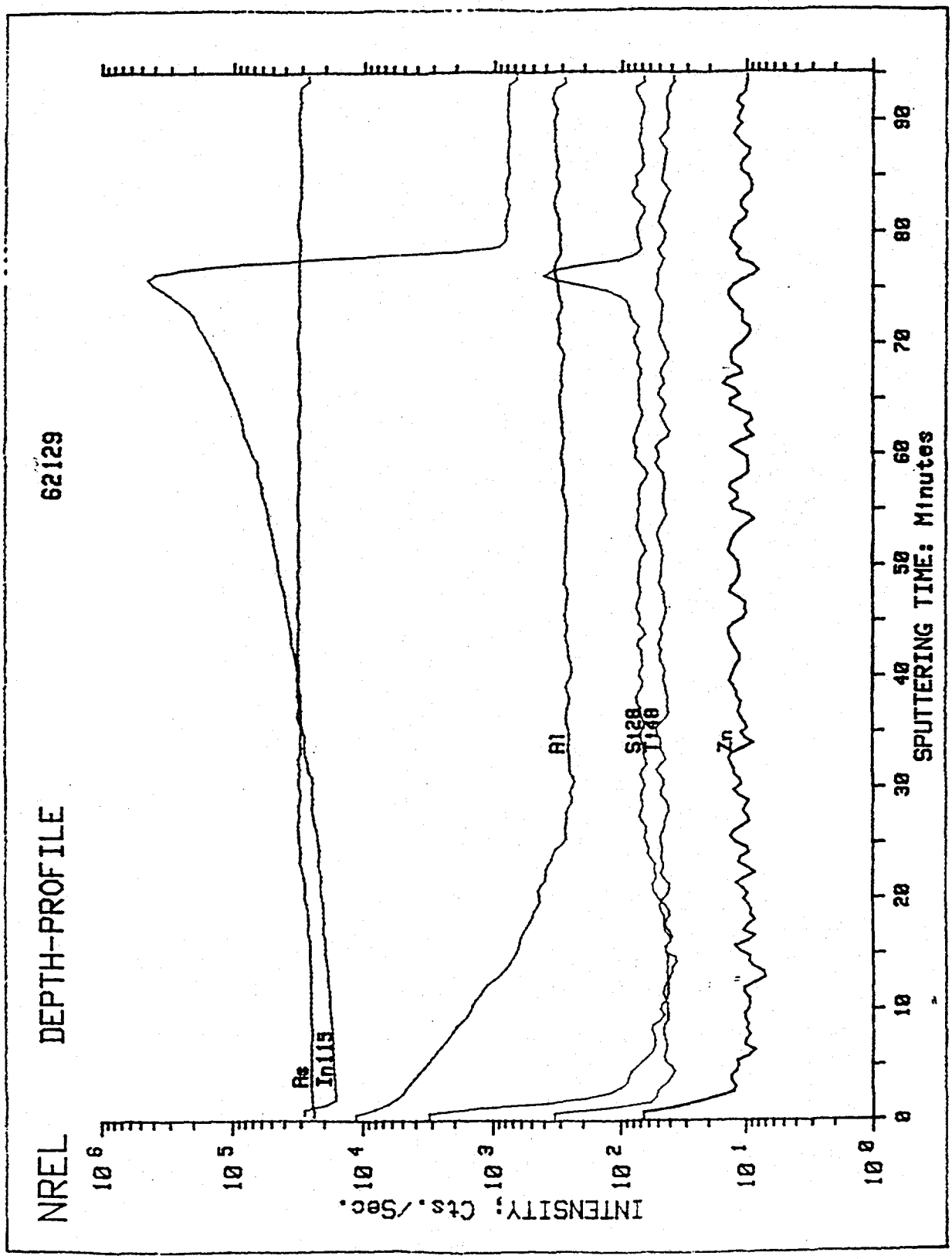


Figure 2.1 SIMS depth profile of a GaAs layer on a GaAs substrate. The layer surface is at the left and the substrate to the right.

reached. This general profile was observed in two other GaAs layers profiled, and is indicative of indium desorption in the reactor or manifold.

This contamination had led to low mobility GaAs material. Liquid nitrogen Hall mobilities were measured in these layers in the 3000 to 11000 cm2/V-s range, with a negative correlation between the level of indium measured by SIMS and mobility. The data for the four GaAs samples profiled is given in Table 1 below. Run numbers 62122, 62128, and 62130 were all runs involving the growth of GaInP; the runs directly following these showed highest indium contamination. The indium counts were observed to drop in the cases of 62132 and 62133, where GaAs growth slowly improved the layer quality in the reactor.

**Table 2.1: GaAs LAYER MOBILITY AND INDIUM CONTAMINATION**

| Run # | 77K Mobility | Indium Counts (Peak) |
|---|---|---|
| 62123 | 3860 cm2/V-s | 400K /s |
| 62129 | 4740 | 500K |
| 62132 | 4700 | 120K |
| 62133 | 10700 | 20K |

With this correlation between mobility and indium, we evaluated various fixes by using the Hall measurement to gauge improvements in the layer. The most clear cut result obtained was the growth of GaAs after cleaning of the reactor walls: a liquid-nitrogen Hall mobility over 40,000 cm2/V-s was achieved. In separate experiments, the susceptor and TMIn source were ruled out as direct causes of the excess indium. The chemistry for the wall reaction is unknown, but we know that there is recirculation above the susceptor. This is attributed to the large volume of the reactor chamber.

High-mobility undoped GaAs layers were reproduced with liquid-nitrogen Hall mobilities over 50,000 cm2/V-s, and room-temperature Hall mobilities over 6,000 cm2/V-s. Doped layers were grown, and undoped layers which followed maintained the high purity levels. Indium was introduced into the reactor and the purity tests reproduced with similar results. GaInP was grown to introduce phosphorus into the reactor and the purity tests reproduced with similar results. Surfaces were specular. Doped layers were calibrated, and lattice matching of the GaInP layers to GaAs substrates reproduced.

## 2.3 Silicon Impurity Effects

As seen in Figure 2.1, there is a silicon spike at the substrate-layer interface. This type of impurity spike is typically due to wafer cleaning procedures, and is not a factor in the type of structures studied here. However, the SIMS measurements did pick up additional silicon spikes, as seen in Figure 2.2. The spike on the right side of the figure, between the GaAs substrate and the GaAs buffer layer, is due to wafer cleaning. The rise in the silicon signal at the second layer of InGaP is characteristic of silicon

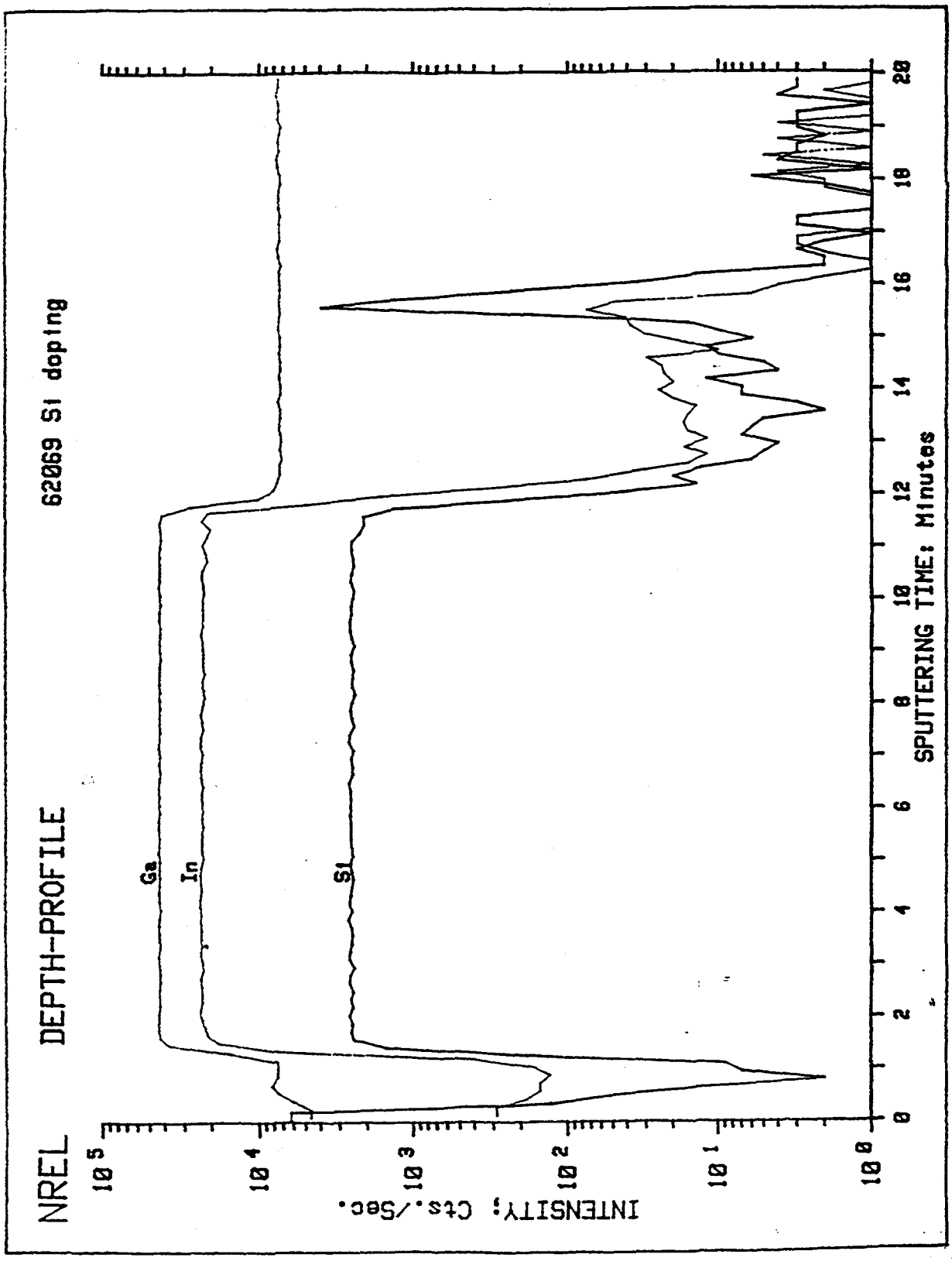


Figure 2.2 SIMS depth profile of a GaInP/GaAs layer on a GaAs substrate. The GaInP layer is at the left and the substrate to the right. Both layers are intentionally undoped.

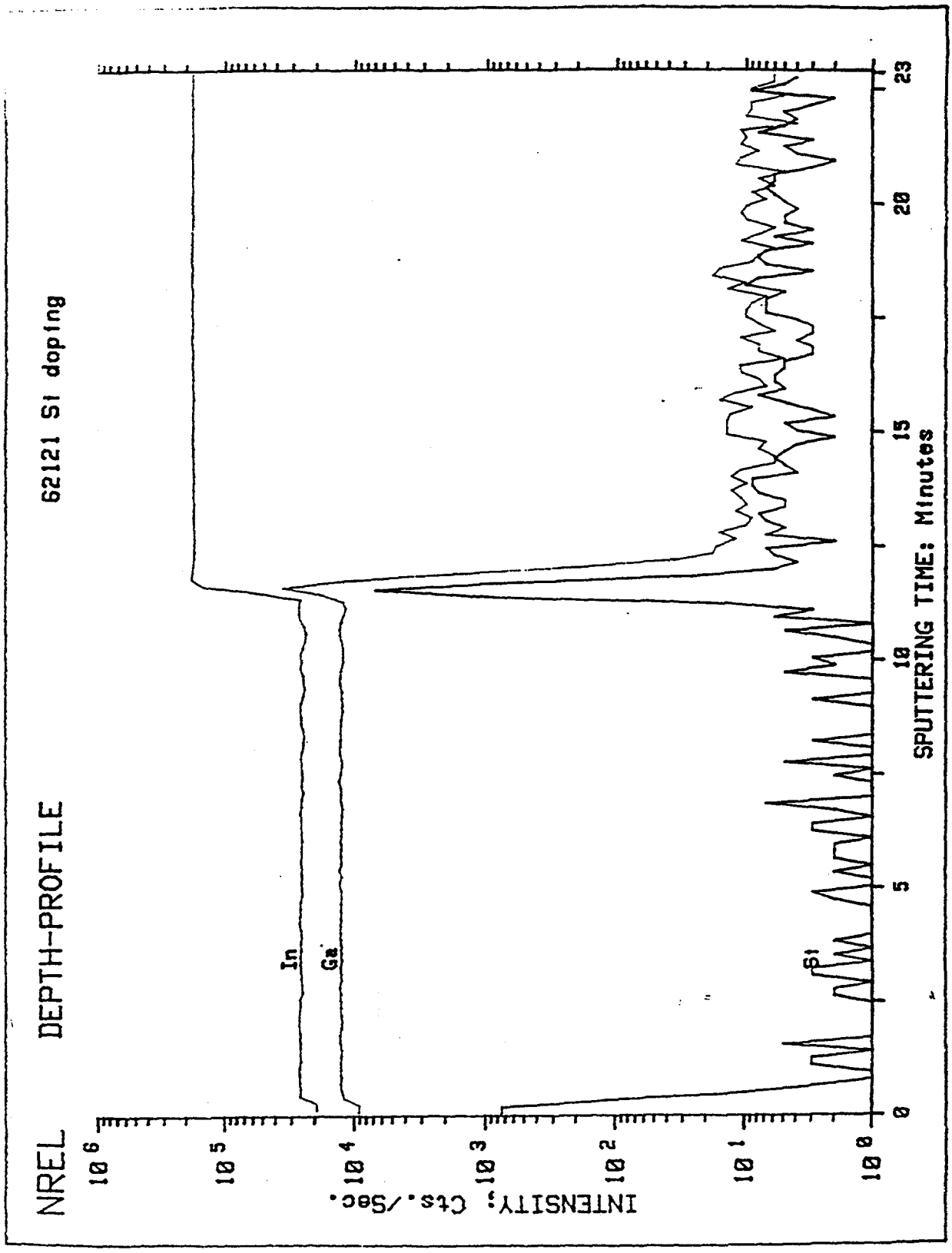


Figure 2.3 SIMS depth profile of a GaInAs layer on an InP substrate. The GaInAs layer is at the left and the substrate to the right. Although the silicon interface spike is present, silicon doping in the GaInAs layer is absent.

impurities in one of the source materials, in this case either In or P as the Si signal did not correlate to the Ga or As prescence. By looking at the SIMS of an InGaAs layer grown on an InP substrate as in Figure 2.3, one can deduce that the silicon correlated with the phosphorus, and was likely introduced into the system as an impurity in the TBP source.

Hall measurements on these samples showed n-type doping in the range of $10^{15}$ to $10^{16}$ $cm^{-3}$, consistent with the SIMS measurements.

## 3. GaInP CELL DEVELOPMENT

Various cell structures were grown to test the effects of the cell components on cell performance. The components tested included emitter thickness and composition, and back-surface field. A matrix of the different structures is shown in Table 3.1 below. The best cell performance resulted from structures with a 0.2 um GaAs emitter under a GaInP window, accompanied by a GaInP back-surface field layer. The external quantum efficiency and illuminated IV curves for one of these cells are shown in Figures 3.1 and 3.2.

**Table 3.1: GaInP/GaAs SOLAR CELL PARAMETERS**

| Run # | Emitter Layer | Emitter Thickness | Contact Thickness | Back-Surface Field Layer |
|---|---|---|---|---|
| 62220 | GaAs | 0.1 | 0.2 | GaInP |
| 62222 | GaAs | 0.2 | 0.2 | GaInP |
| 62224 | GaAs | 0.2 | 0.4 | GaInP |
| 62225 | GaAs | 0.2 | 0.2 | GaAs |
| 62226 | GaInP | 0.1 | 0.2 | GaInP |
| 62227 | GaInP | 0.2 | 0.2 | GaInP |

The quantum efficiency is improved from our earlier cell experiments, but indicates several areas for cell current collection improvement. The peak efficiency is 0.88 at 530 nm, and drops off to about 0.7 at the band edge. This shape suggests that the GaAs base material quality could be improved. Postulating that the GaInP back-surface field (BSF) layer was causing a problem with the base layer, we grew the same structure without the GaInP BSF layer. Cells fabricated without the heterojunction BSF exhibited poorer red response, indicating that the GaInP BSF was beneficial for current collection. Further tests are necessary.

The efficiency of these cells is also limited by the fill factor. As seen in Figure 3.2, the low fill is due to a series resistance in the cell. Emitter thickness strongly affected both current collection and fill factor, pointing to additional optimization of the emitter for higher efficiencies. However, the interfaces between the GaInP and the GaAs layers is not well characterized, and may contribute to the cell resistance.

GaInP emitters were investigated by the growth and fabrication of heterojunction cells. These cells had 0.1 and 0.2 um GaInP emitters grown directly on the GaAs base, with GaInP BSF layers. The cells exhibited current loss in the short-wavelength spectrum, indicative of either absorption in the emitter or high surface recombination at the emitter-contact layer interface.

Sample: 62222−7 Temperature = 25.0°C

May. 29, 1992 10:08 am Area used = 0.808 cm²

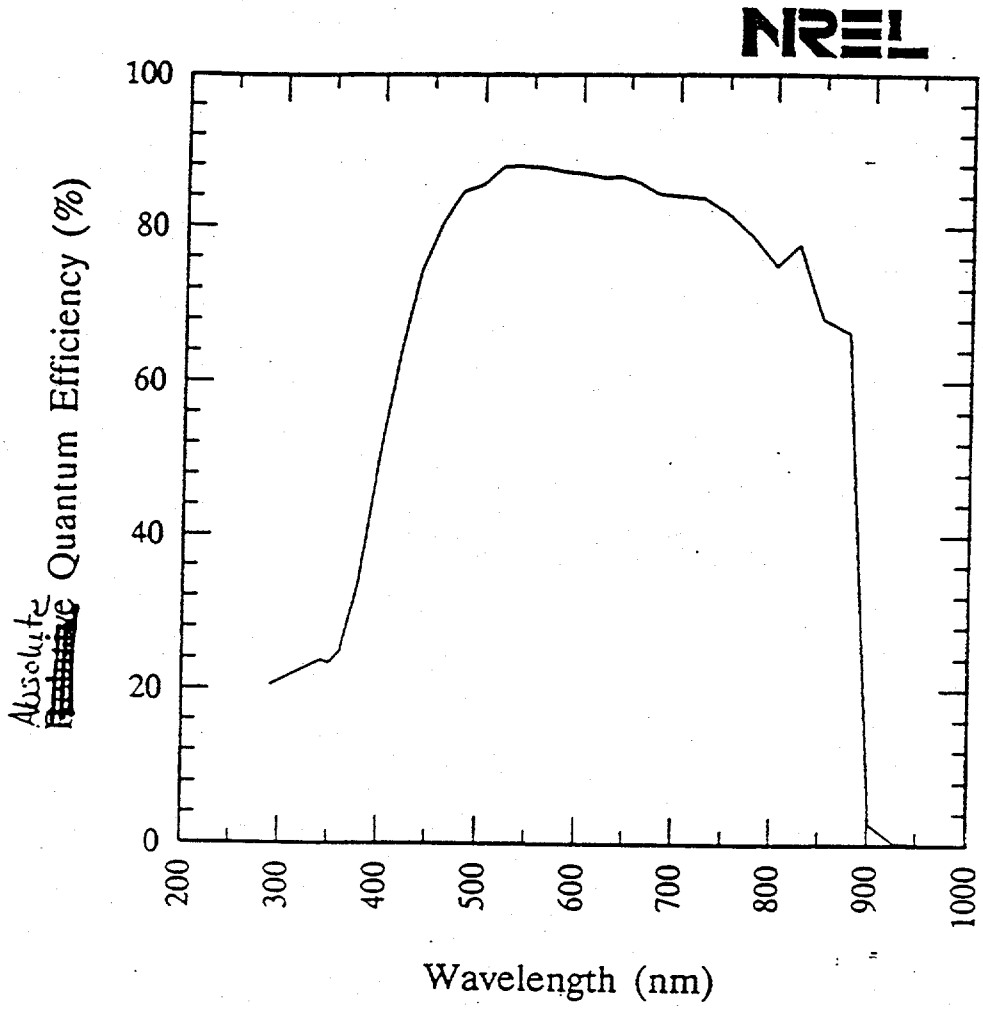


Light bias = 5.00 mA

Zero voltage bias

Figure 3.1. External quantum efficiency of a GaInP/GaAs solar cell. The cell was measured with 5.0 mA light bias, and zero voltage bias.

Sample: 62222−7 Temperature = 25.0°C

Jun. 1, 1992 3:53 pm Area = 0.808 cm²

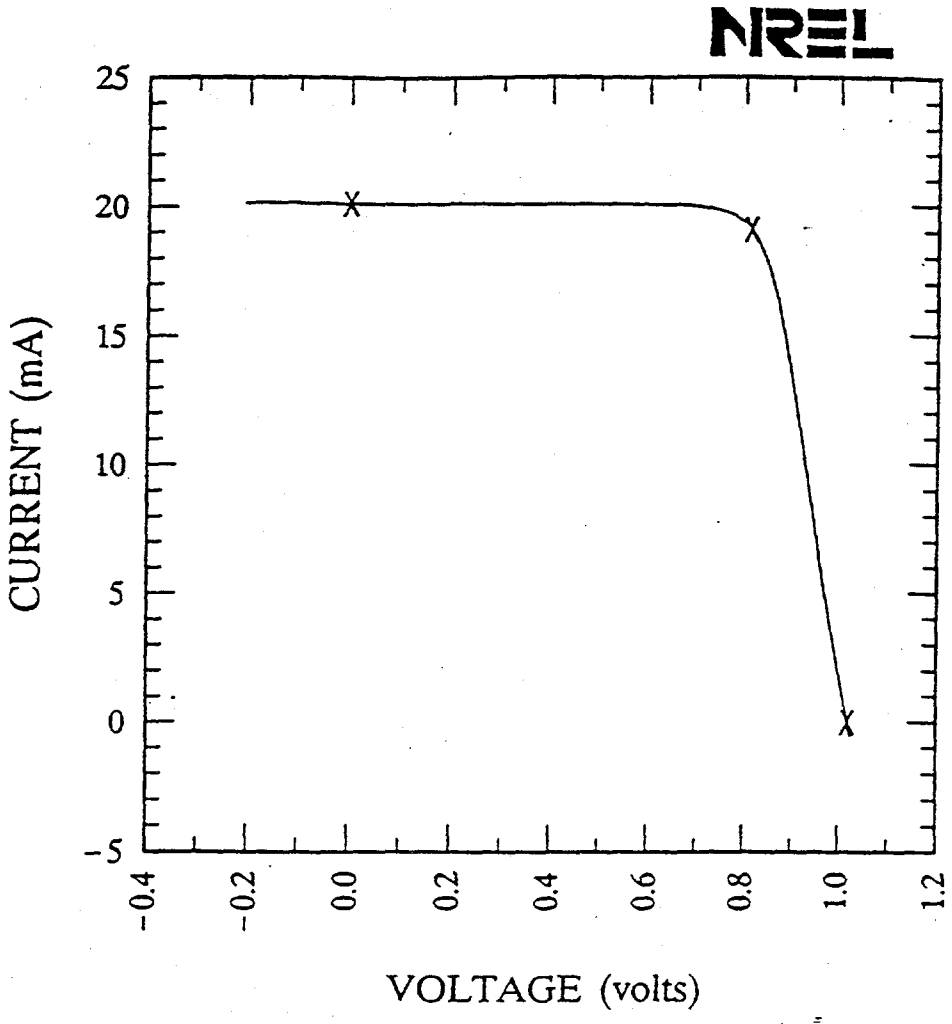


| | |
|---|---|
| $V_{oc}$ = 1.020 volts | $I_{sc}$ = 20.11 mA |
| $J_{sc}$ = 24.89 mA/cm² | $P_{max}$ = 15.55 mW |
| Fill factor = 75.82 % | $I_{max}$ = 19.13 mA |
| Efficiency = 19.2 % | $V_{max}$ = 0.8130 V |

Figure 3.2. I-V curve for the cell of Figure 3.1, under simulated AM1.5 illumination.

## 4. ORGANOMETALLIC OVERGROWTH

Conditions for the in situ overgrowth by OMCVD were determined and continuous GaAs layers were grown over a separation mask layer. To enhance the overgrowth ratio and inhibit heterogeneous nucleation, HCl was added to the reactor during growth. Several of these layers have subsequently been successfully cleaved from their substrates.

### 4.1 Screening for HCl

Overgrowth conditions were investigated using a screening experiment. Controlled factors were the arsine flow (50 to 100 sccm), HCl flow (400 to 1200 sccm), TMGa flow (6 to 12 sccm), growth temperature (540 to 640 C), and growth pressure (90 to 130 torr). Responses were the overgrowth ratio, growth rate, and nucleation on the overgrowth mask. The experiment was designed with the commercial software package RS1. The experimental specifications are given in Table 4.1 below. The objective was screening, using a fractional-factorial design. Overgrowth ratios from 0 to 2 were observed with layers growing at from 0.4 to 9 um/hour. Nucleation was measured in areas away from the overgrowth lines.

**Table 4.1: HCl - EXPERMENTAL SPECIFICATIONS**

| Description | Value |
|---|---|
| # Controlled factors | 5 |
| Objective | Screening |
| Model Type | Interactions |
| Design Type | Fractional-Factorial |
| Centerpoints | 2 |
| Number of Runs | 18 |
| Number of Blocks | 1 |
| Run Order | Random |

Nucleation, overgrowth ratio, and growth rate were modeled over the parameter space. Overgrowth ratio turned out to be a complex function of all five factors (independent variables in the matrix). The linear terms were not as significant as the interactions. The maximum overgrowth occurred near the high value of the five factors, but the interesting result was that with the interactions, all of the factors had an impact on the overgrowth ratio. The significance of the interaction terms is that each factor became important in one or more regions of parameter space. This result is somewhat counter productive as the objective of the screening experiment was to eliminate factors from further consideration. Details are given in the sections below.

The effects of these interactions can be seen in contourplots of the responses as a function of two of the factors, where values for the other three factors are held fixed. Thus the contourplot is essentially a two-dimensional slice of the five-dimentional parameter space. Figure 4.1 is a contourplot showing nucleation and overgrowth ratio as functions of pressure

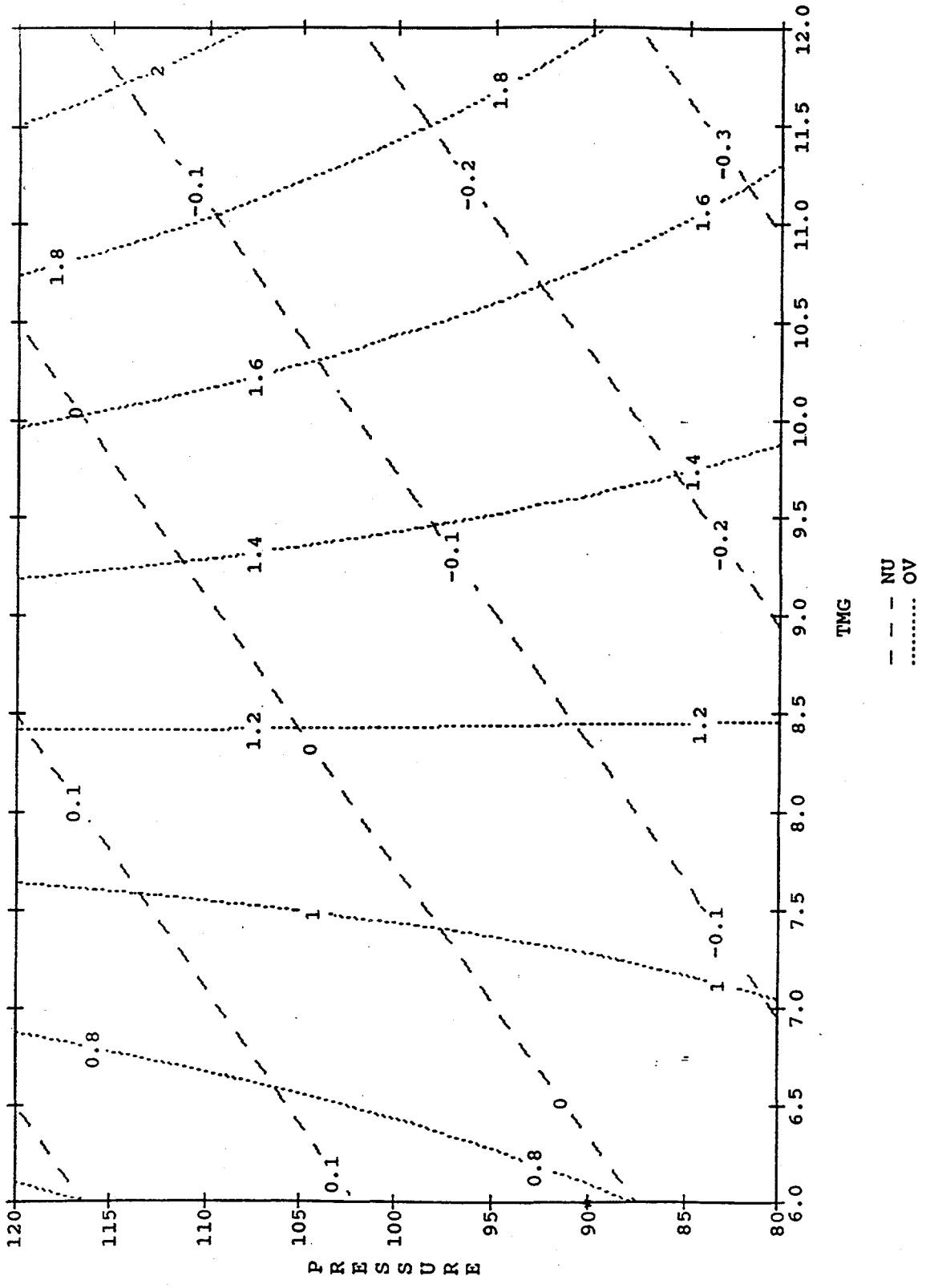


Figure 4.1 Contourplot of nucleation and overgrowth ratio as functions of pressure and TMGa flow. The fixed factor values were 100 for arsine flow, 1200 for HCl flow, and 640 C for temperature.

and TMGa flow. The nucleation density modelled was low over the entire space, which was expected as the HCl flow was fixed high. The curves were generated from the models, so that the negative values for nucleation density indicate no nucleation. The overgrowth ratio increased with the increase in TMGa flow, while an increase in pressure improved the ratio only at the high values for TMGa flow.

Figure 4.2 is another contourplot, showing growth rate and overgrowth ratio as functions of pressure and HCl flow. The effect of the HCl on growth rate is clear: the more HCl, the lower the growth rate. The overgrowth ratio also increases for the higher HCl flow, as well as for the higher pressure.

There are an infinite number of plots that may be generated from this experiment, but to identify the key effects, we have looked at the main and interactive effects. These plots are given in the following sections, with their implication on overgrowth for CLEFT processing summarized in Section 4.5.

## 4.2 Nucleation

Nucleation on the mask was relatively rare in the matrix, being driven by increases in reactor pressure and temperature as much as by reduction in HCl flow. Since the only nucleation occurred at low values for HCl flow, temperature, and TMGa flow, nucleation turned out to not be a constraint on the overgrowth conditions.

The main effects graph for nucleation is shown in Figure 4.3. The five factors are listed on the left, along with their variation. The main effect of each of these factors on nucleation (NU) was plotted with 95% confidence intevals. Nucleation was in units of $cm^{-3}$, while the flows (Arsine, Hydrogen chloride, and Trimethylgallium) are in units of sccm (cubic centimeters per minute at standard temperature and pressure), temperature T is degrees Centigrade, and pressure P is torr. The increase in HCl flow tended to reduce nucleation, while increases in reactor pressure or temperature tended to increase nucleation. Arsine and TMGa flow showed no main effect. However, as mentioned above the interactions were significant.

There were four interaction terms for nucleation: HCl flow and temperature, HCl flow and pressure, temperature and pressure, and TMGa flow and arsine flow. These interaction effects are plotted in Figures 4.2 to 4.5. The following is a summary of the effects on nucleation; where unstated, there were no significant effects found.

Increasing HCl flow reduces nucleation at higher temperatures.
Increasing HCl flow reduces nucleation at higher pressures.
Increasing temperature increases nucleation at lower HCl flows.
Increasing temperature increases nucleation at higher pressures.
Increasing pressure increases nucleation at higher temperatures.
Increasing pressure increases nucleation at lower HCl flows.
Increasing TMGa flow increases nucleation at lower arsine flows, while decreasing nucleation at higher arsine flows.
Increasing arsine flow increases nucleation at lower TMGa flows, while decreasing nucleation at higher TMGa flows.

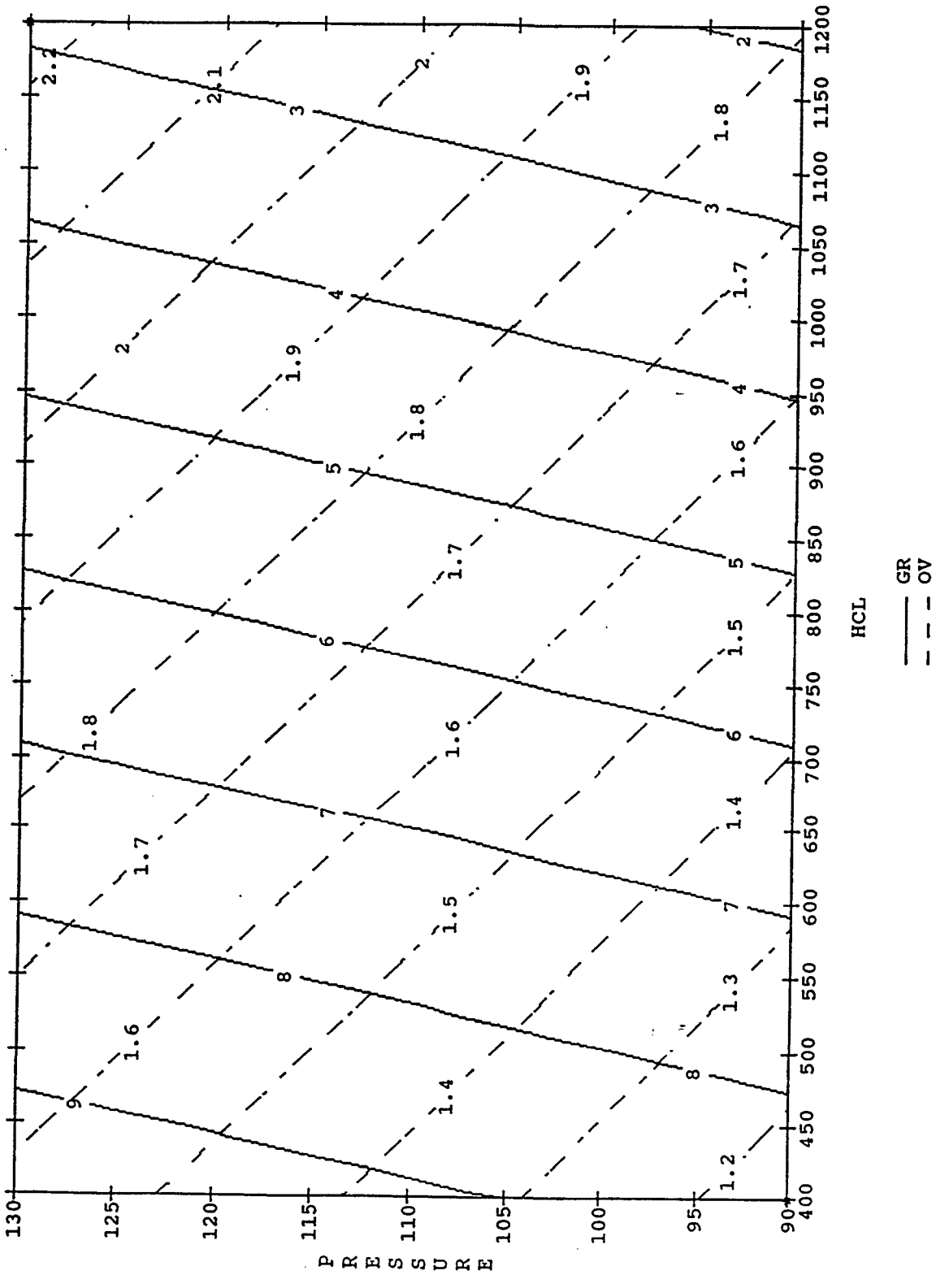


Figure 4.2 Contourplot of growth rate and overgrowth ratio as functions of pressure and HCl flow. The fixed factor values were 100 for arsine flow, 12 for TMGa flow, and 640C for temperature.

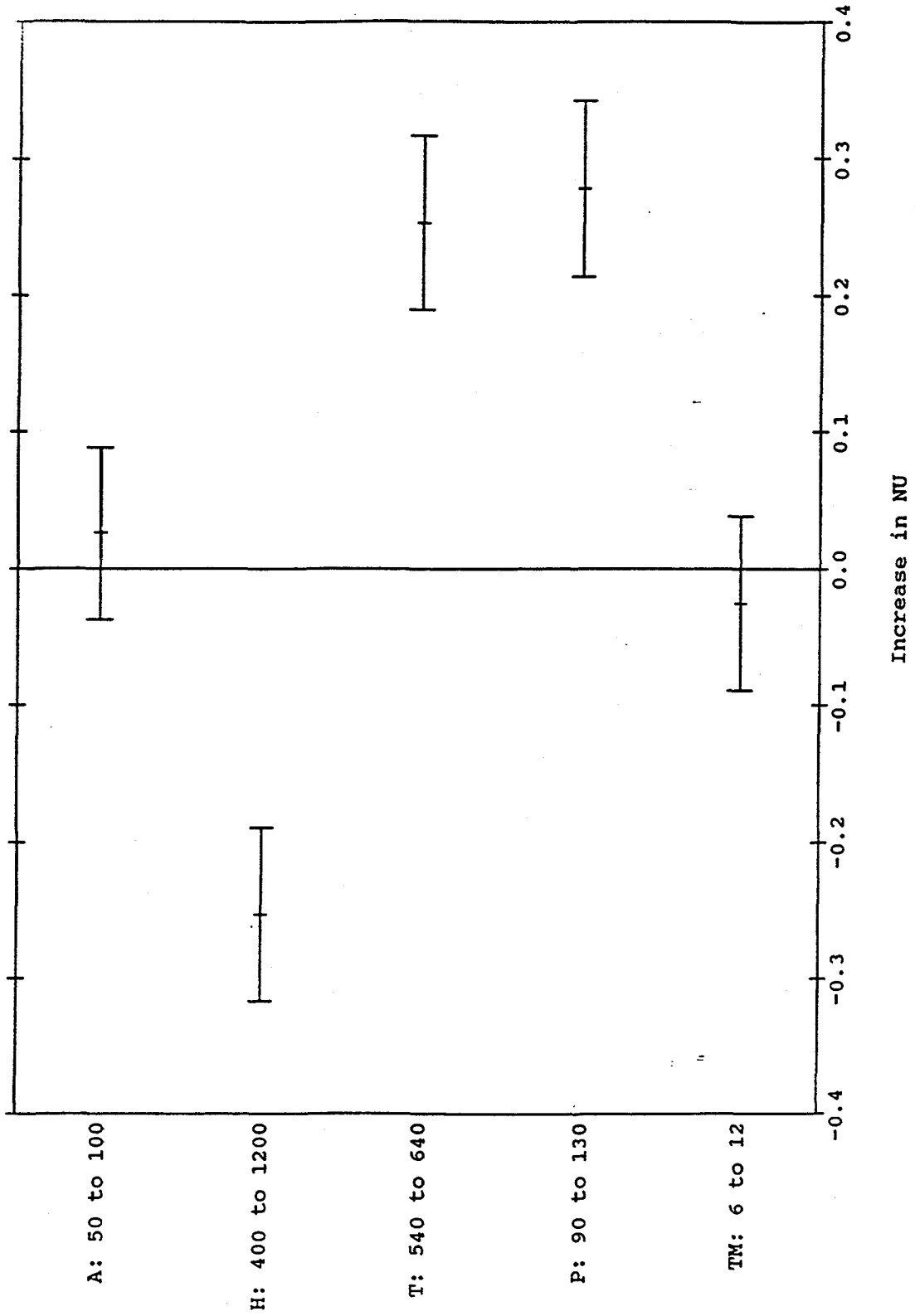


Figure 4.3 Main effects for nucleation. The five factors are listed on the left, along with their variation, are arsine flow (A), hydrogen chloride flow (H), trimethylgallium flow (TM), temperature (T), and pressure (P).

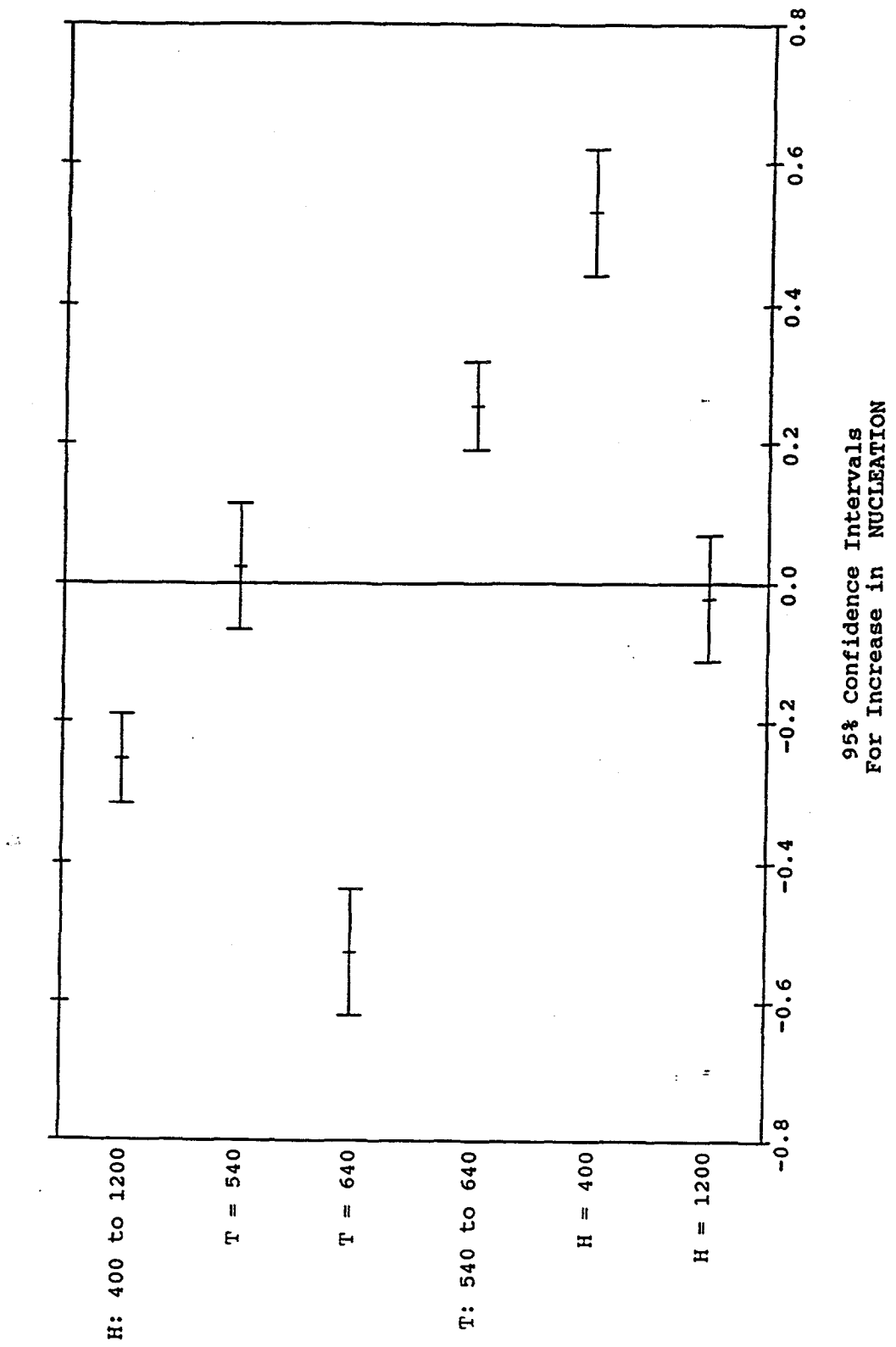


Figure 4.4 Interactive effects of HCl flow with temperature on nucleation.

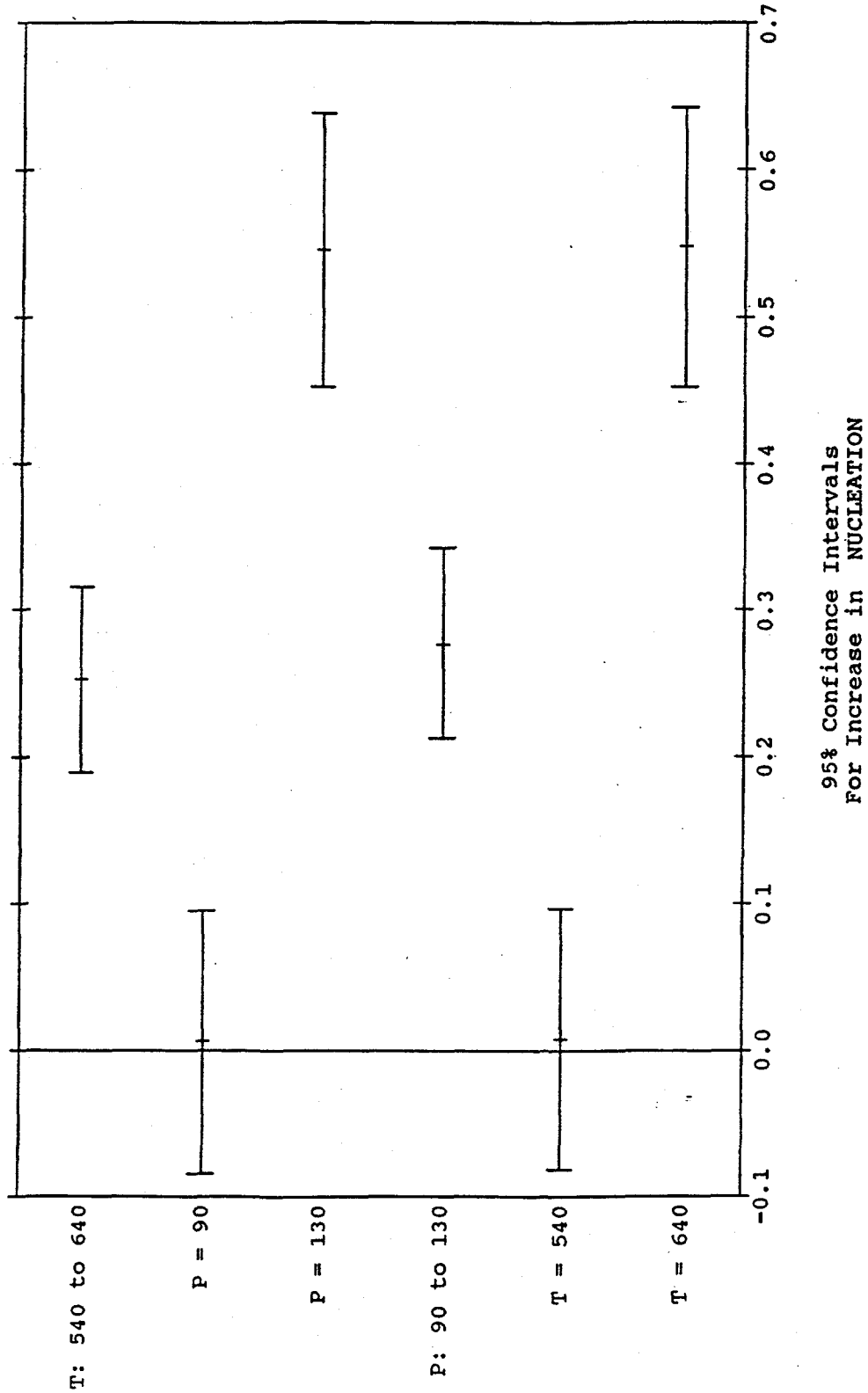


Figure 4.5 Interactive effects of temperature with pressure on response nucleation.

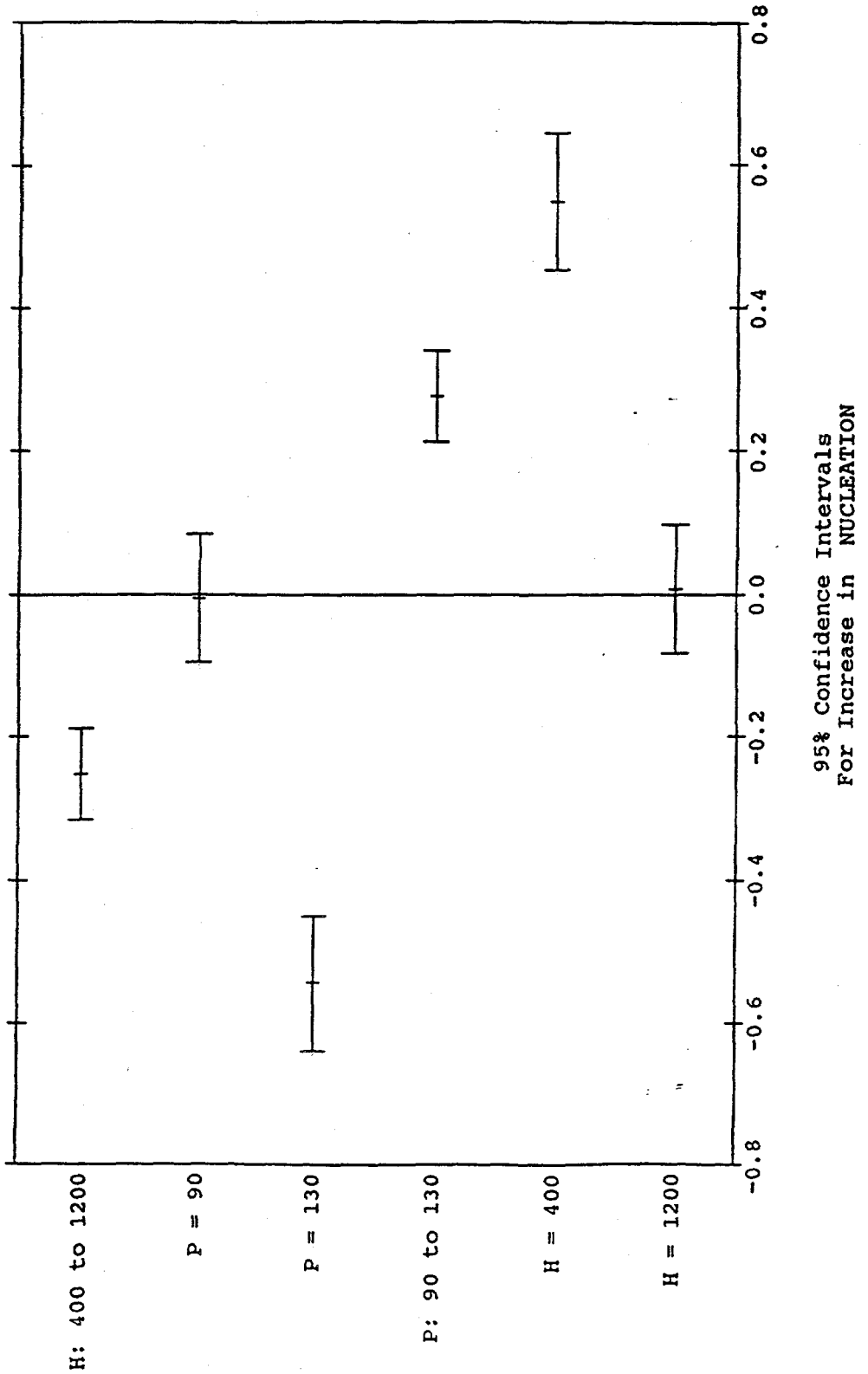


Figure 4.6 Interactive effects of HCl flow with pressure on response nucleation.

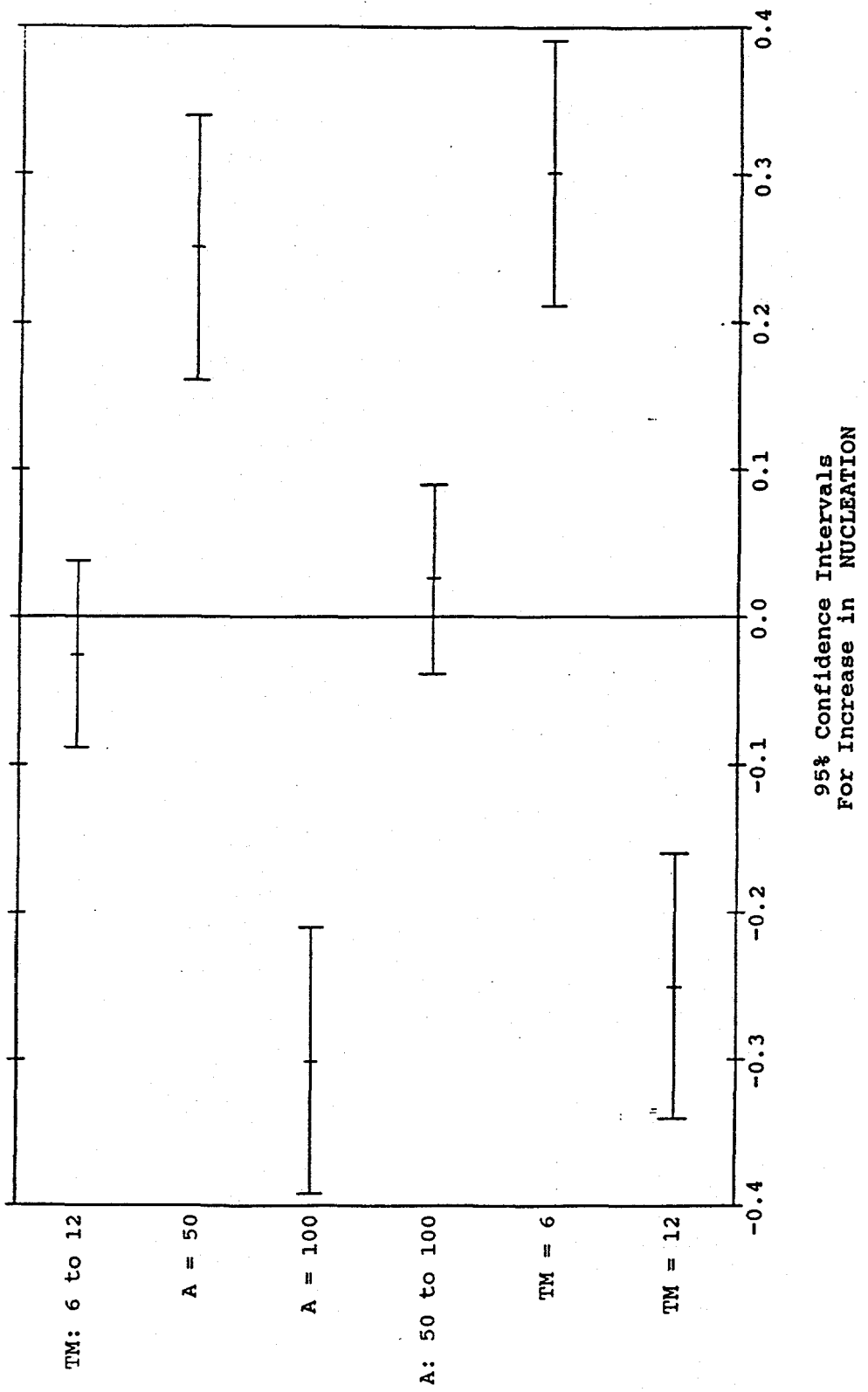


Figure 4.7 Interactive effects of TMGa flow with arsine flow on response nucleation.

## 4.3 Overgrowth Ratio

Main effects and interactive effects plots for the overgrowth ratio are given in Figures 4.8 through 4.17, roughly in order of significance. The main effets plot of Figure 4.8 only indicates higher overgrowth for higher TMGa flows and lower pressure, but all of the other factors actually play a role. These interactive effects are summarized below.

Increasing TMGa flow increases overgrowth ratio at higher temperature, while decreases overgrowth ratio at lower temperature.
Increasing temperature increases overgrowth ratio at higher TMGa flow, while decreases overgrowth ratio at lower TMGa flow.
Increasing TMGa flow increases overgrowth ratio at higher HCl flow.
Increasing HCl flow increases overgrowth ratio at higher TMGa flow, while decreases overgrowth ratio at lower TMGa flow.
Increasing temperature increases overgrowth ratio at higher arsine flow, while decreases overgrowth ratio at lower arsine flow.
Increasing arsine flow increases overgrowth ratio at higher temperature, while decreases overgrowth ratio at lower temperature.
Increasing TMGa flow increases overgrowth ratio at higher pressure.
Increasing pressure decreases overgrowth ratio at lower TMGa flow.
Increasing HCl flow increases overgrowth ratio at higher TMGa flow, while decreases overgrowth ratio at lower TMGa flow.
Increasing TMGa flow increases overgrowth ratio at higher HCl flow.
Increasing temperature increases overgrowth ratio at higher pressure.
Increasing pressure decreases overgrowth ratio at lower temperature.
Increasing TMGa flow increases overgrowth ratio at higher arsine flow.

## 4.4 Growth Rate

Growth rate of GaAs on the witness bulk piece was most affected by the HCl flow, decreasing for the higher flow conditions. This decrease even dominated the size of the increase in growth rate with the doubling of the TMGa flow. Main effects and interactive effects plots for the overgrowth ratio are given in Figures 4.18 through 4.22, roughly in order of significance. The main effects plot of Figure 4.18 only indicates significant lower growth rate higher HCl flows, but as in the case of overgrowth ratio, all of the other factors actually play a role. These interactive effects are summarized below.

Increasing HCl flow decreases growth rate at higher temperature.
Increasing temperature increases growth rate at lower HCl flow.
Increasing HCl flow decreases growth rate at higher TMGa flow.
Increasing TMGa flow increases growth rate at lower HCl flow.
Increasing temperature increases growth rate at lower arsine flow.
Increasing arsine flow increases growth rate at lower temperature.
Increasing TMGa flow increases growth rate at higher temperature.

The effect of growth rate on the time to overgrow a CLEFT mask pattern is discussed in the next section.

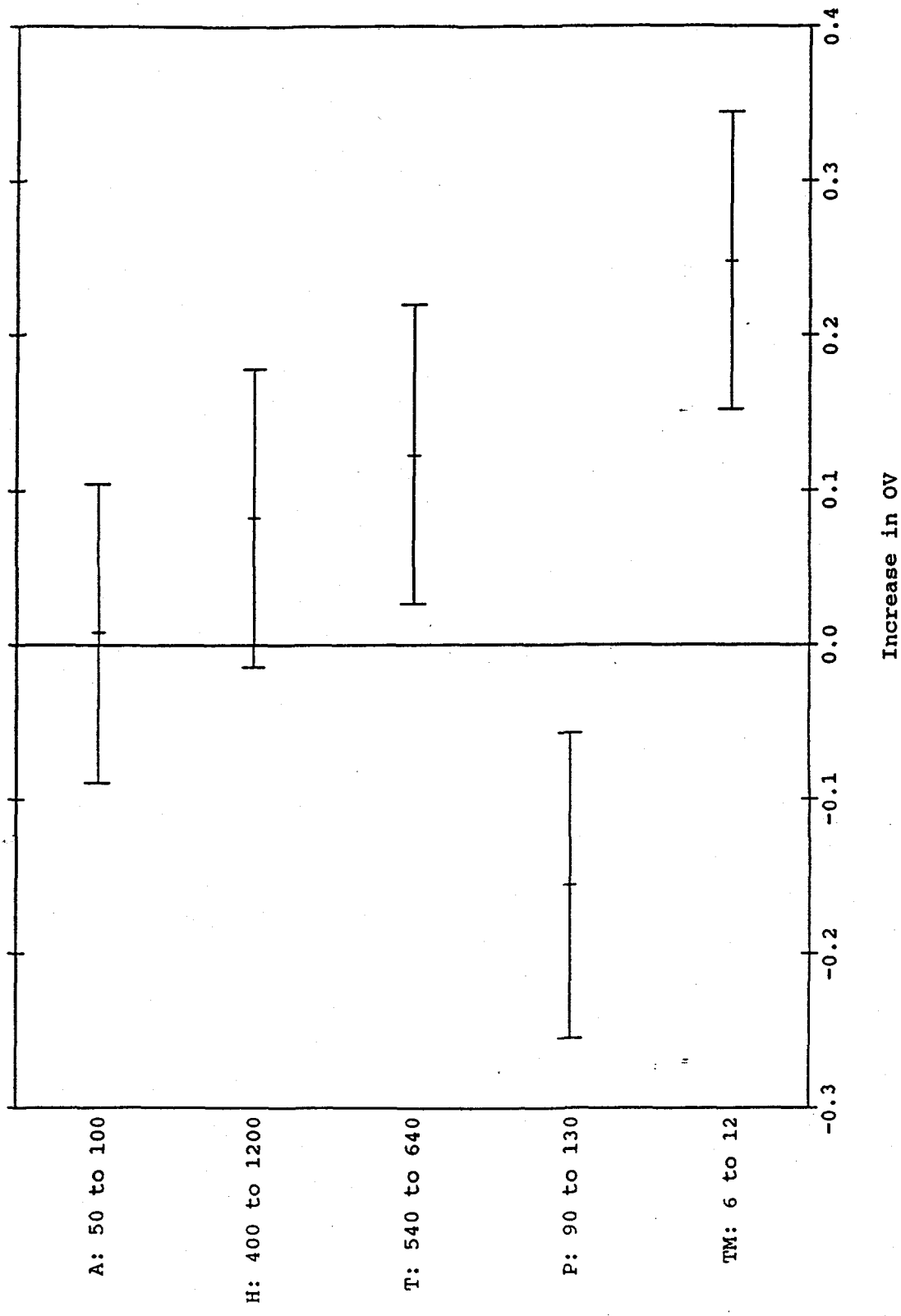


Figure 4.8 Main effects on overgrowth ratio OV. The five factors are listed on the left, along with their variation, are arsine flow (A), hydrogen chloride flow (H), trimethylgallium flow (TM), temperature (T), and pressure (P).

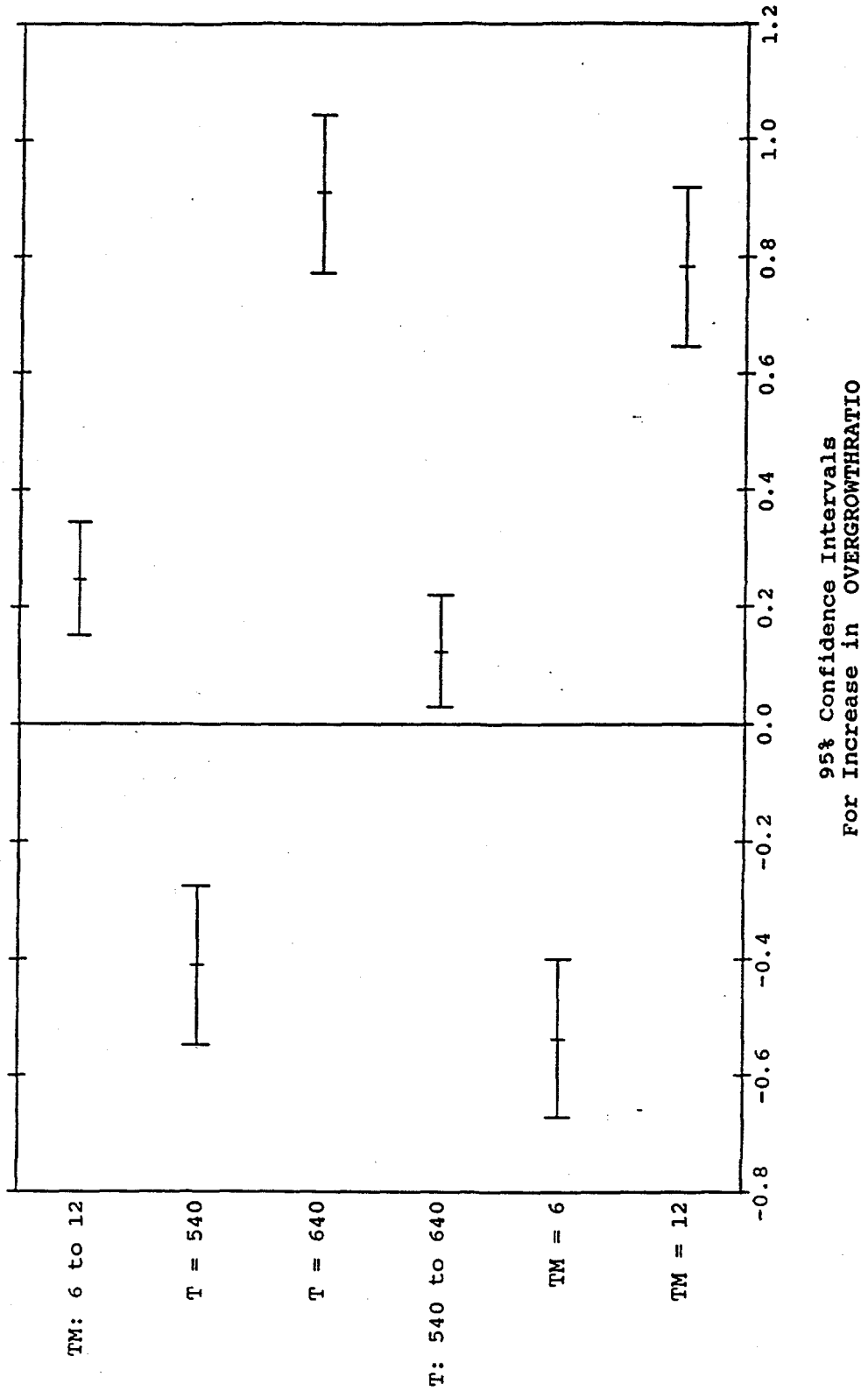


Figure 4.9 Interactive effects of TMGa flow with temperature on response overgrowth ratio.

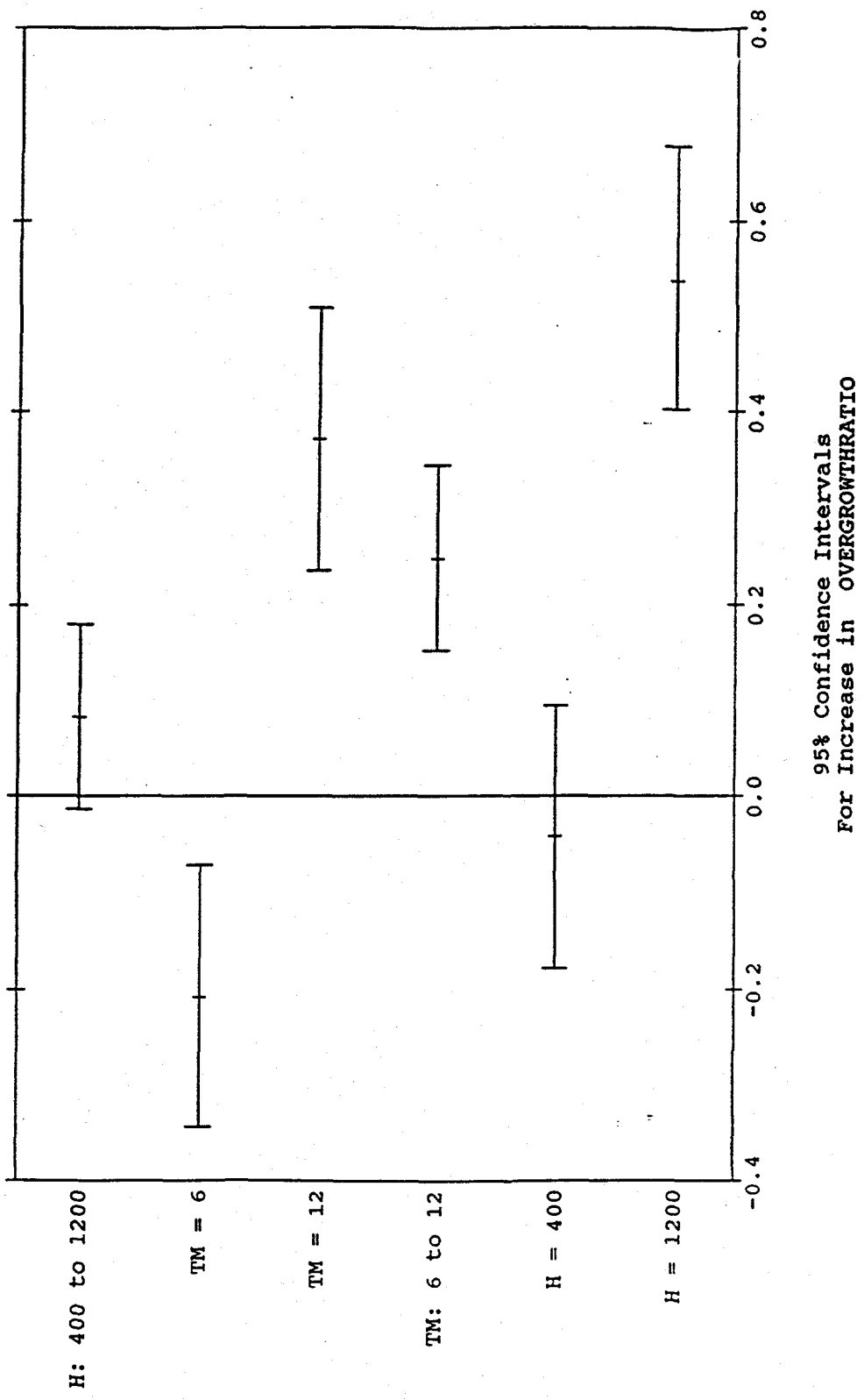


Figure 4.10 Interactive effects of HCl flow with TMGa flow on response overgrowth ratio.

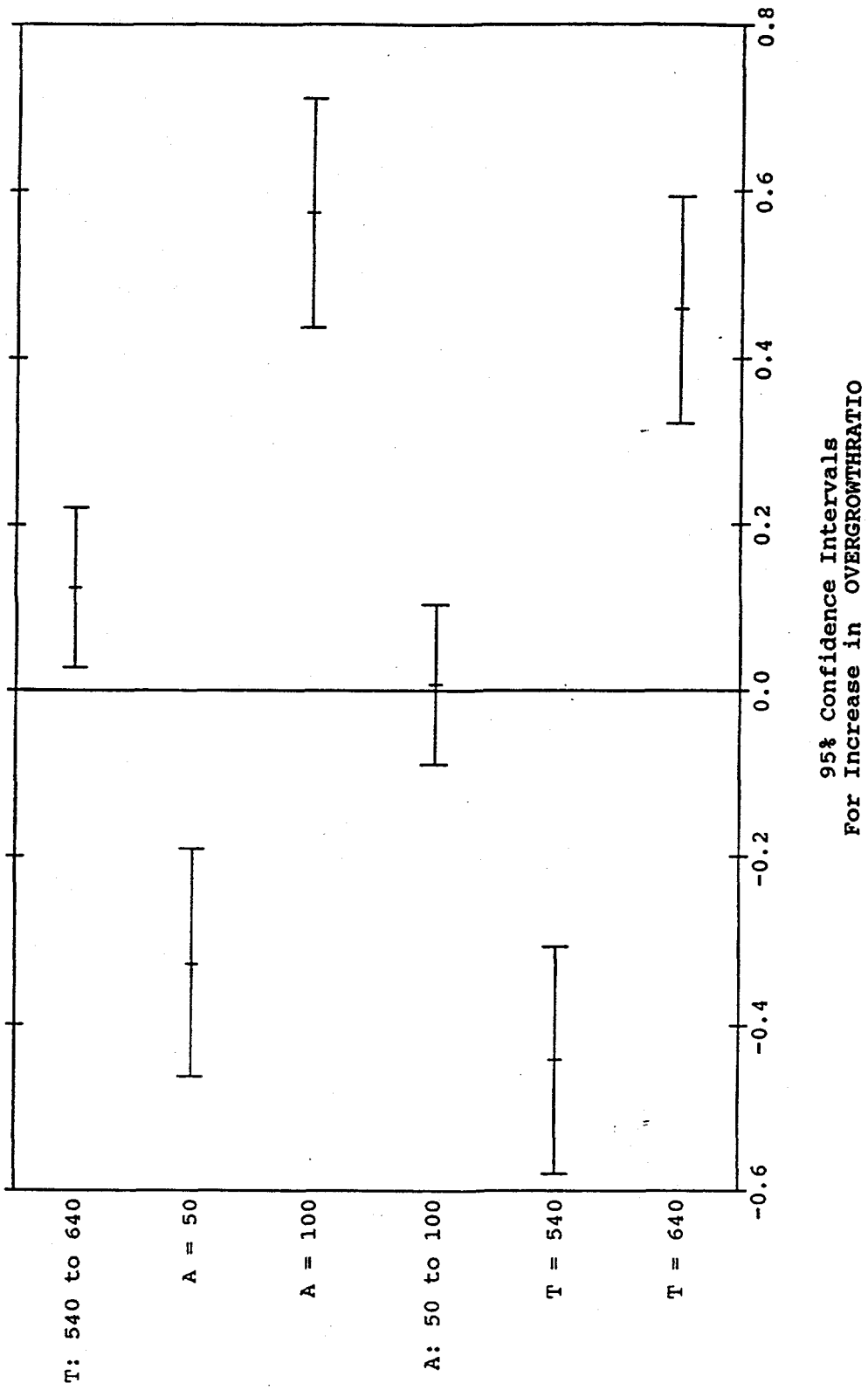


Figure 4.11 Interactive effects of temperature with arsine flow on response nucleation.

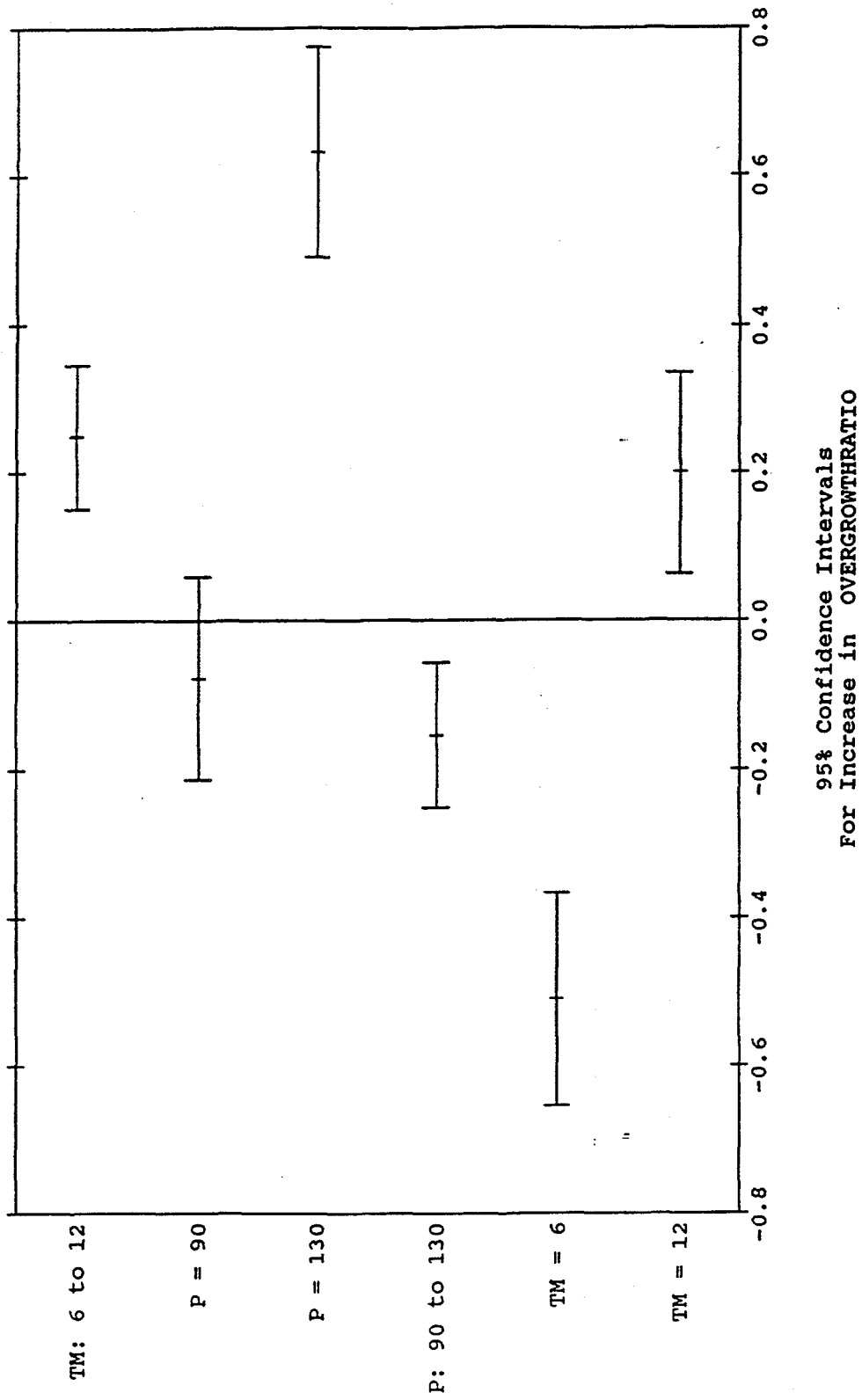


Figure 4.12 Interactive effects of TMGa flow with pressure on response nucleation.

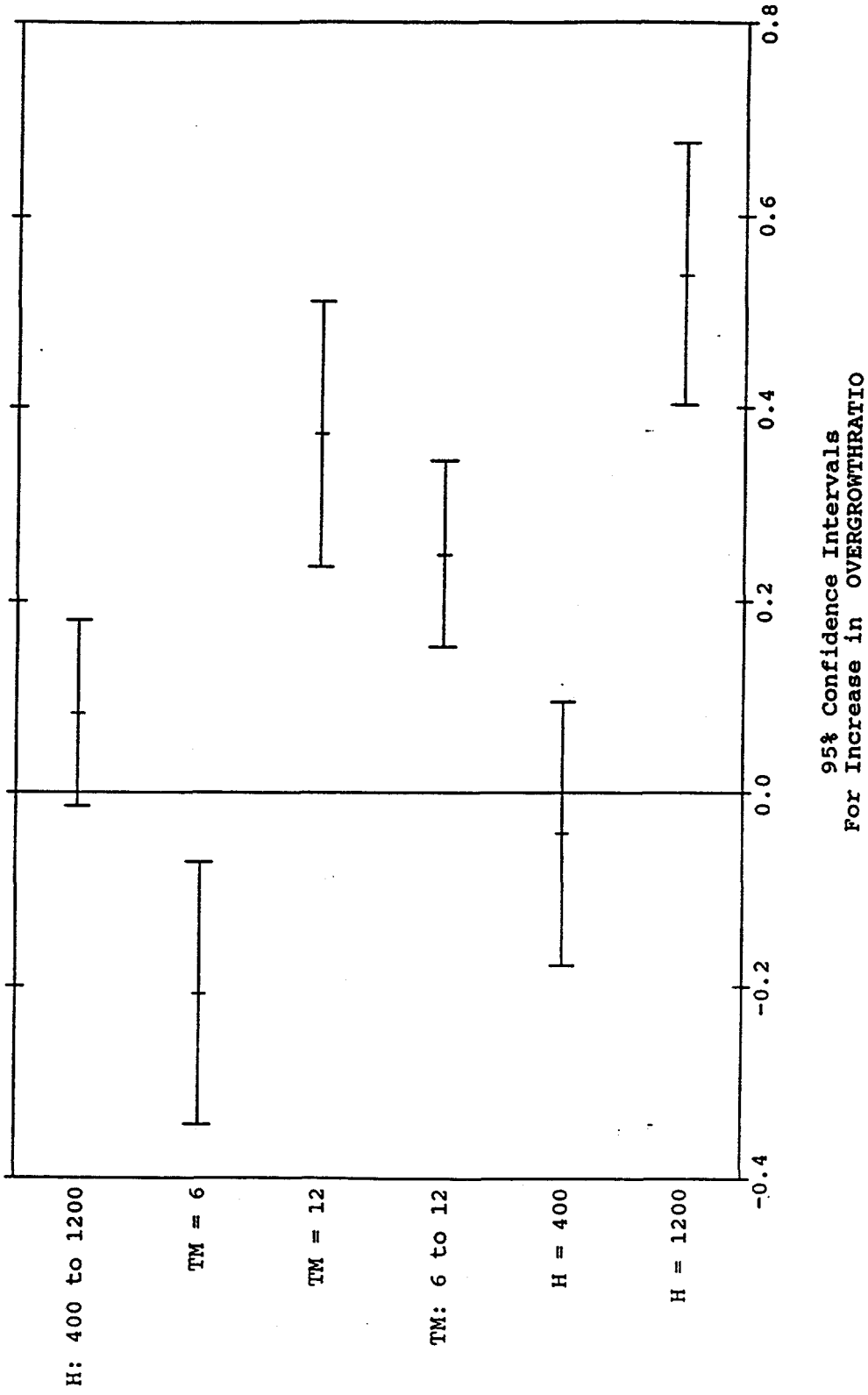


Figure 4.13 Interactive effects of HCl flow with TMGa flow on response nucleation.

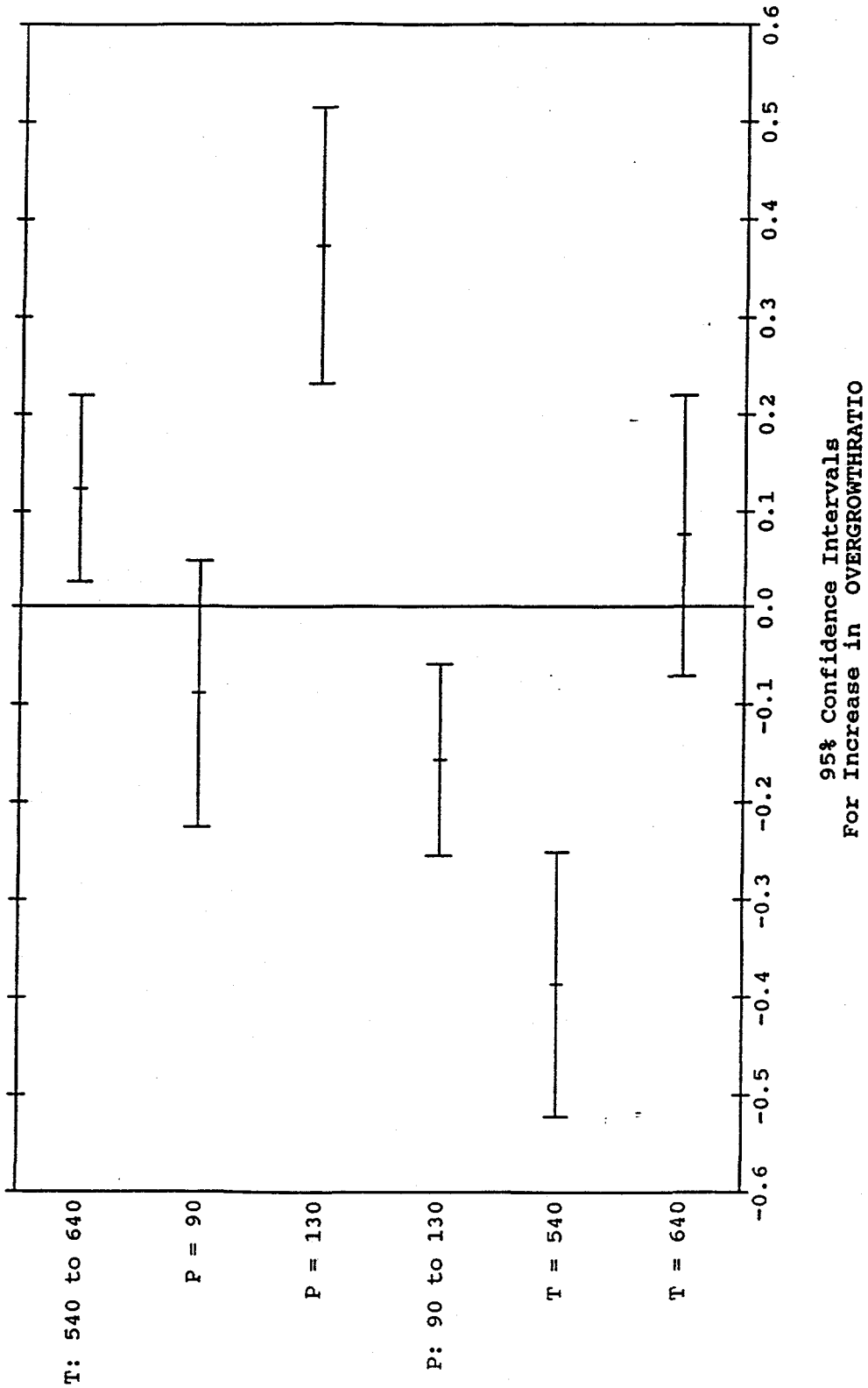


Figure 4.14 Interactive effects of temperature with pressure on response nucleation.

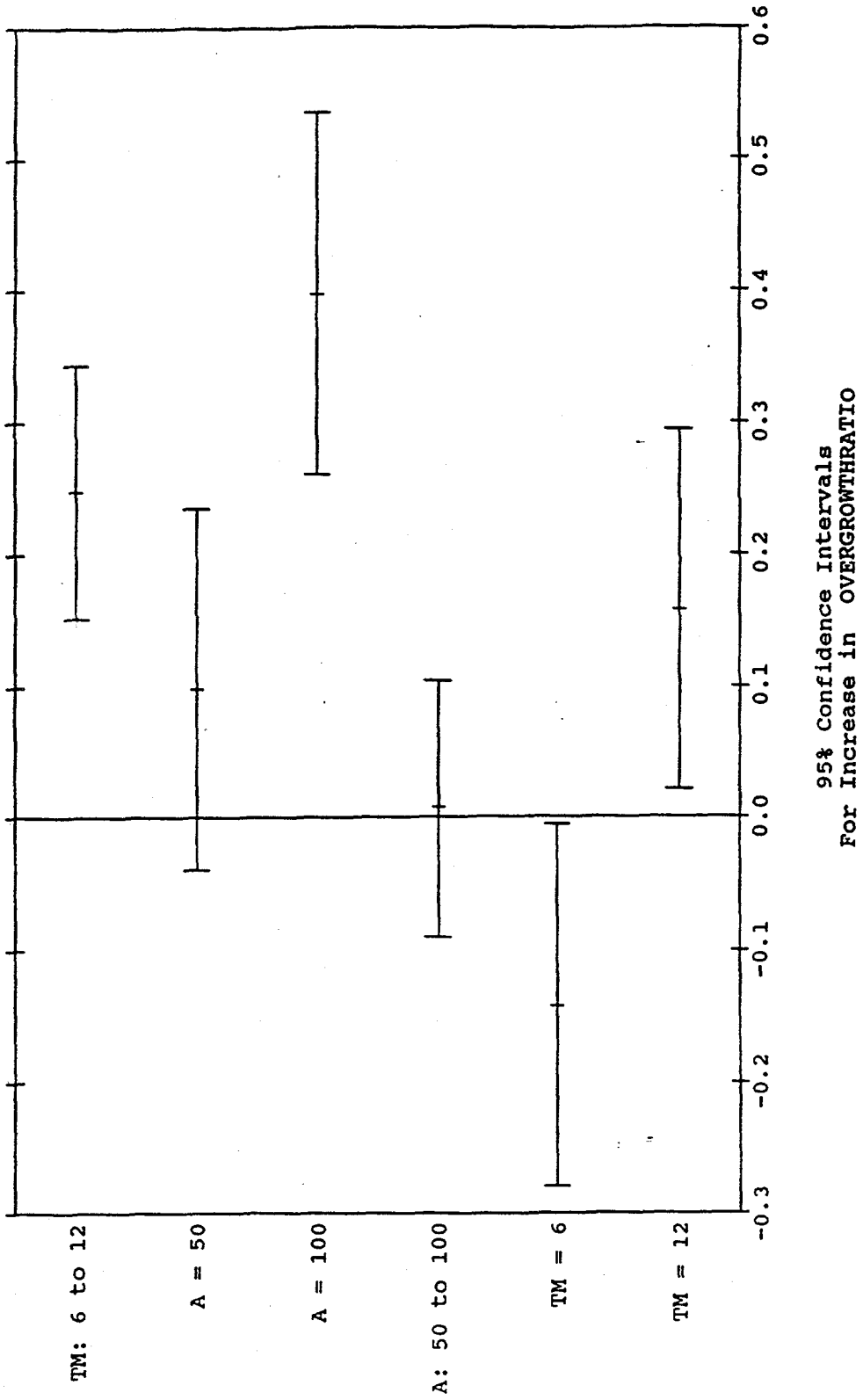


Figure 4.15 Interactive effects of TMGa flow with arsine flow on response nucleation.

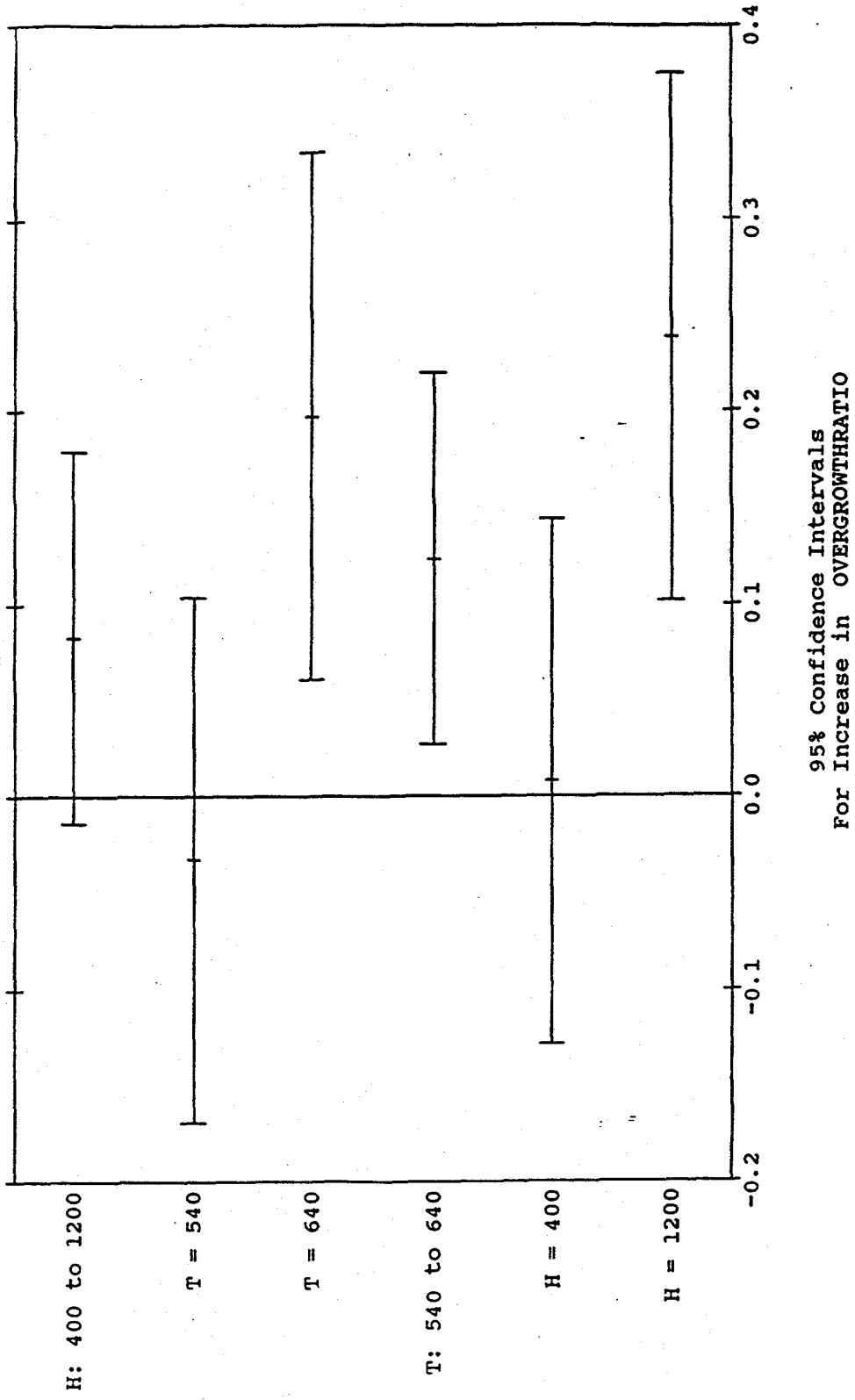


Figure 4.16 Interactive effects of HCl flow with temperature on response nucleation.

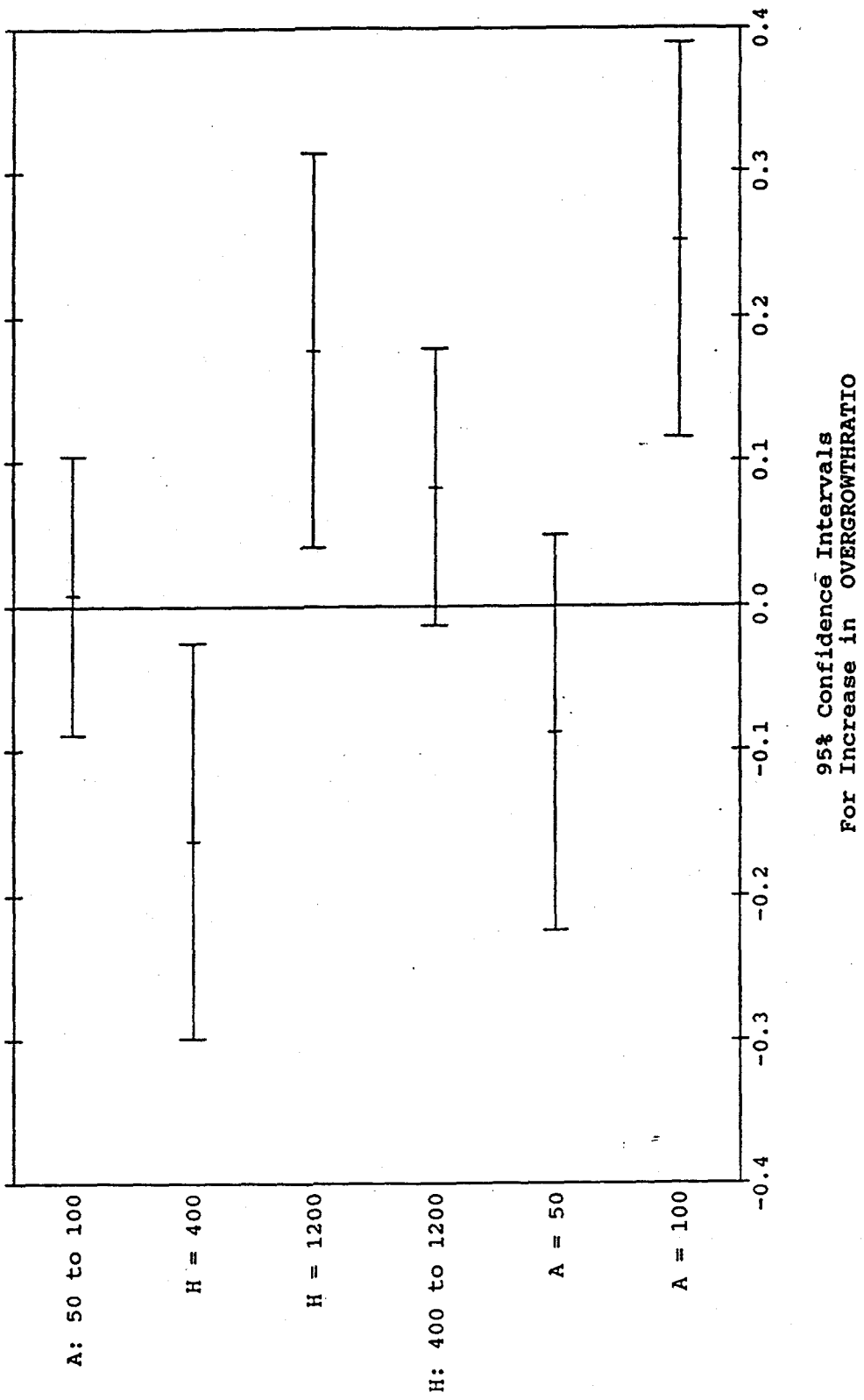


Figure 4.17 Interactive effects of arsine flow with HCl flow on response nucleation.

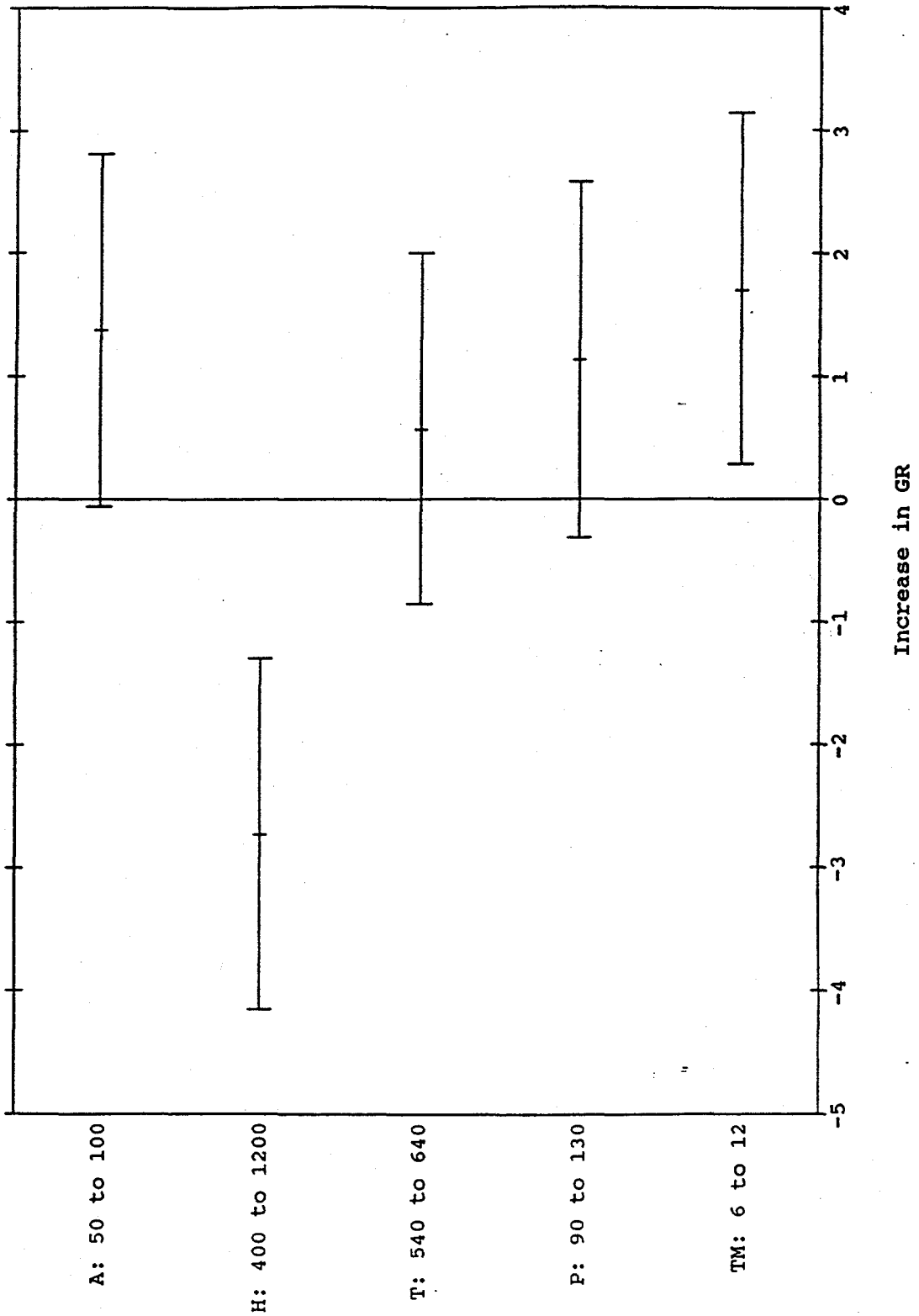


Figure 4.18 Main effects on response growth rate. The five factors are listed on the left, along with their variation, are arsine flow (A), hydrogen chloride flow (H), trimethylgallium flow (TM), temperature (T), and pressure (P).

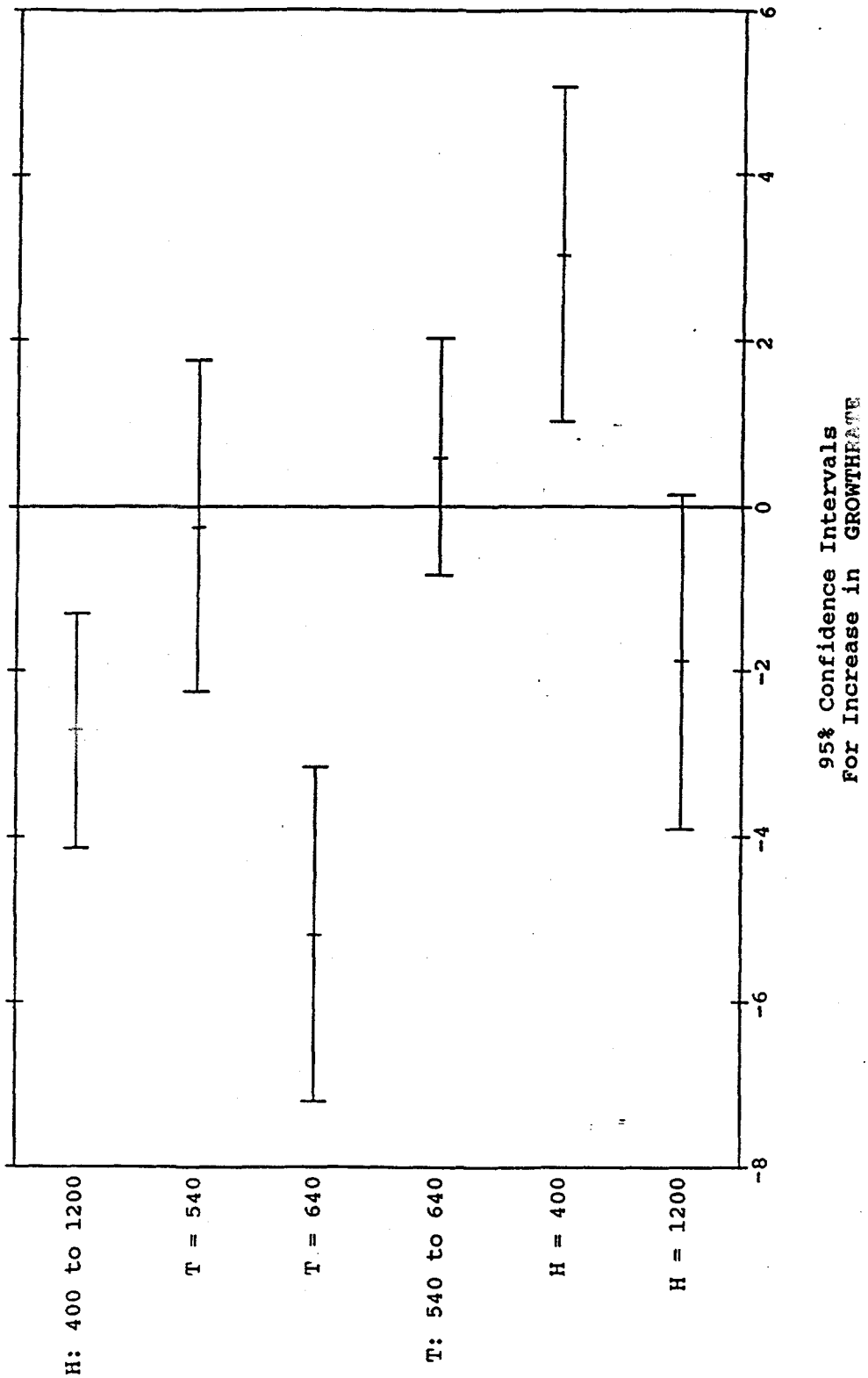


Figure 4.19 Interactive effects of HCl flow with temperature on response growth rate.

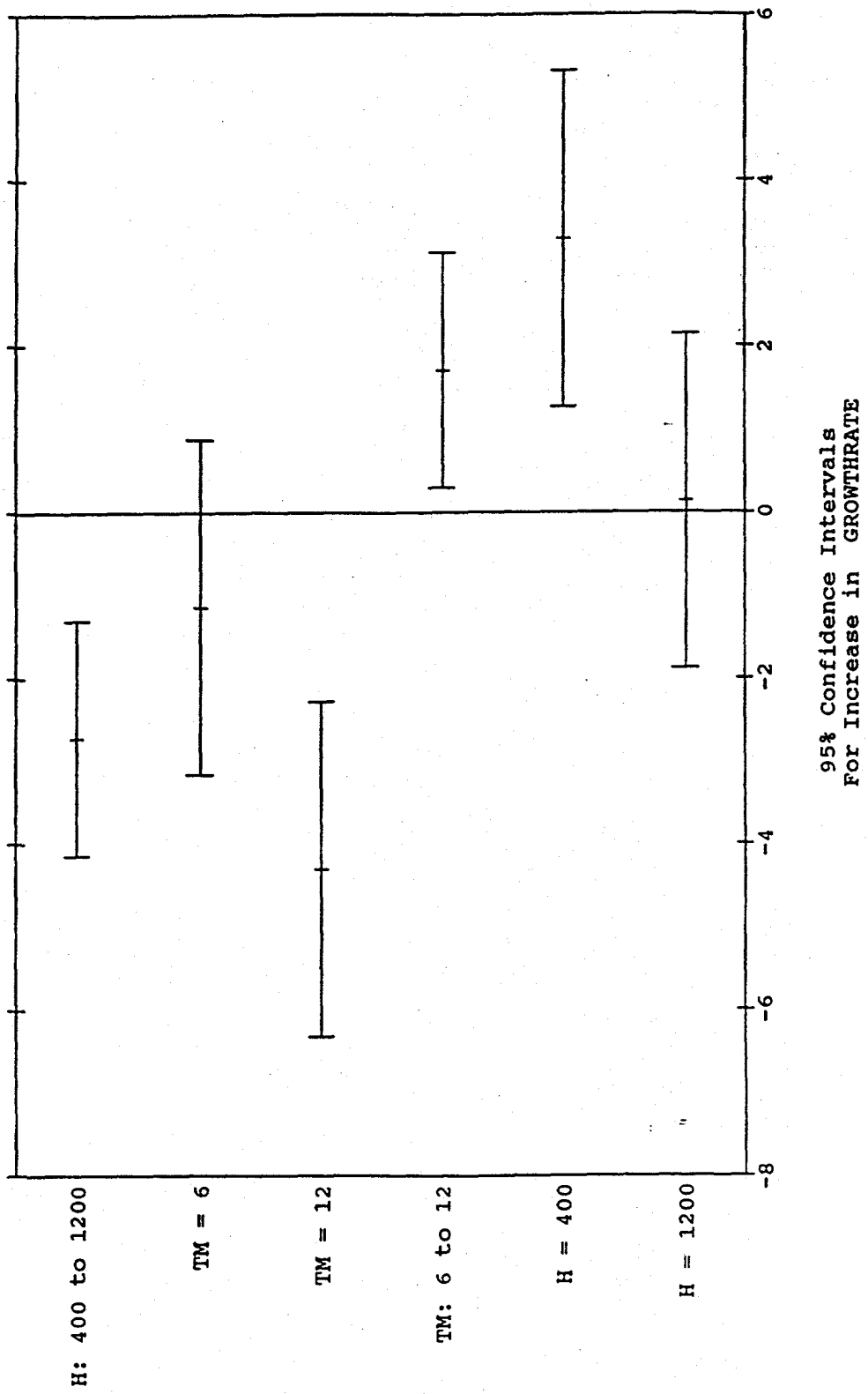


Figure 4.20 Interactive effects of HCl flow with TMGa flow on response growth rate.

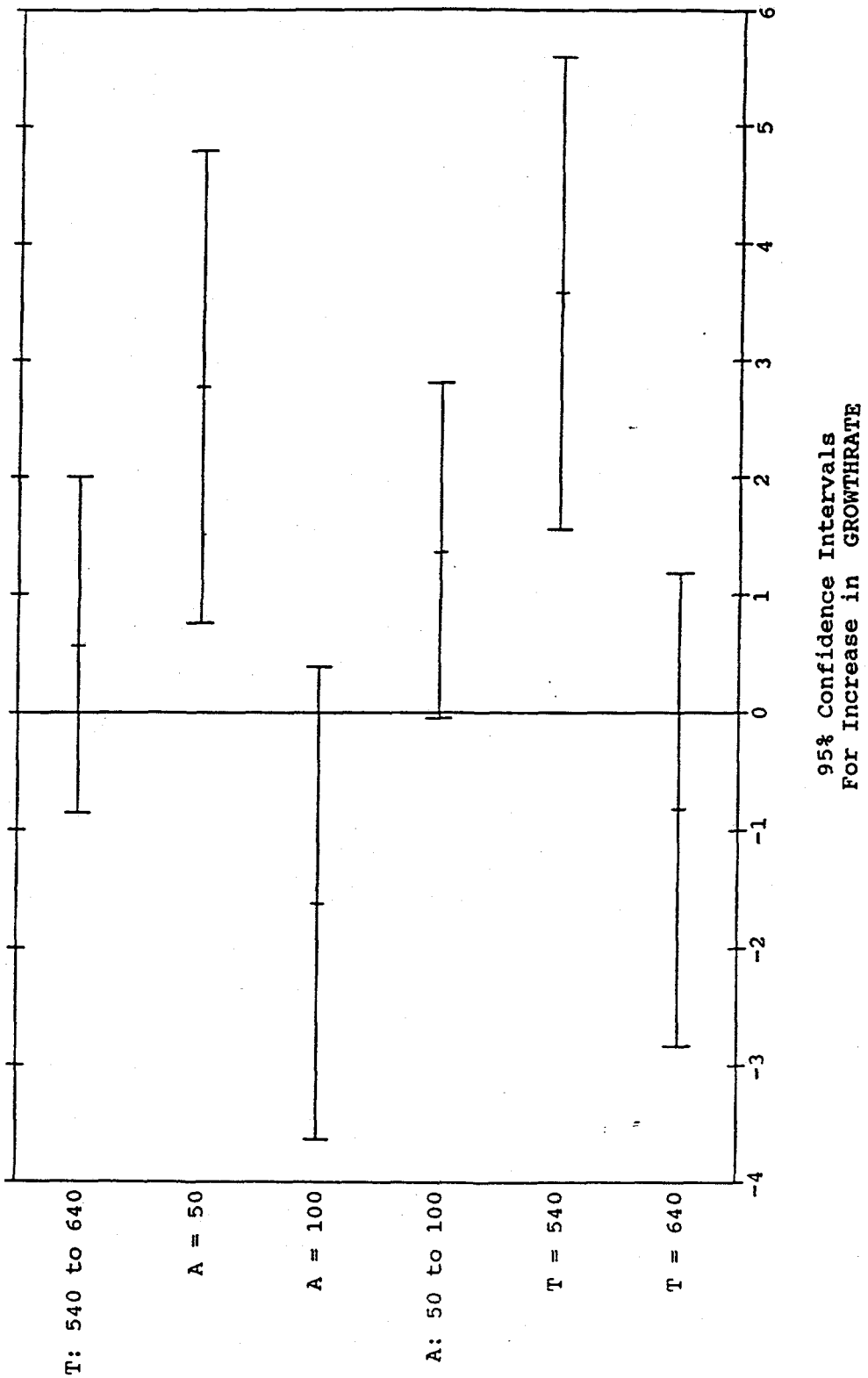


Figure 4.21 Interactive effects of temperature with arsine flow on response growth rate.

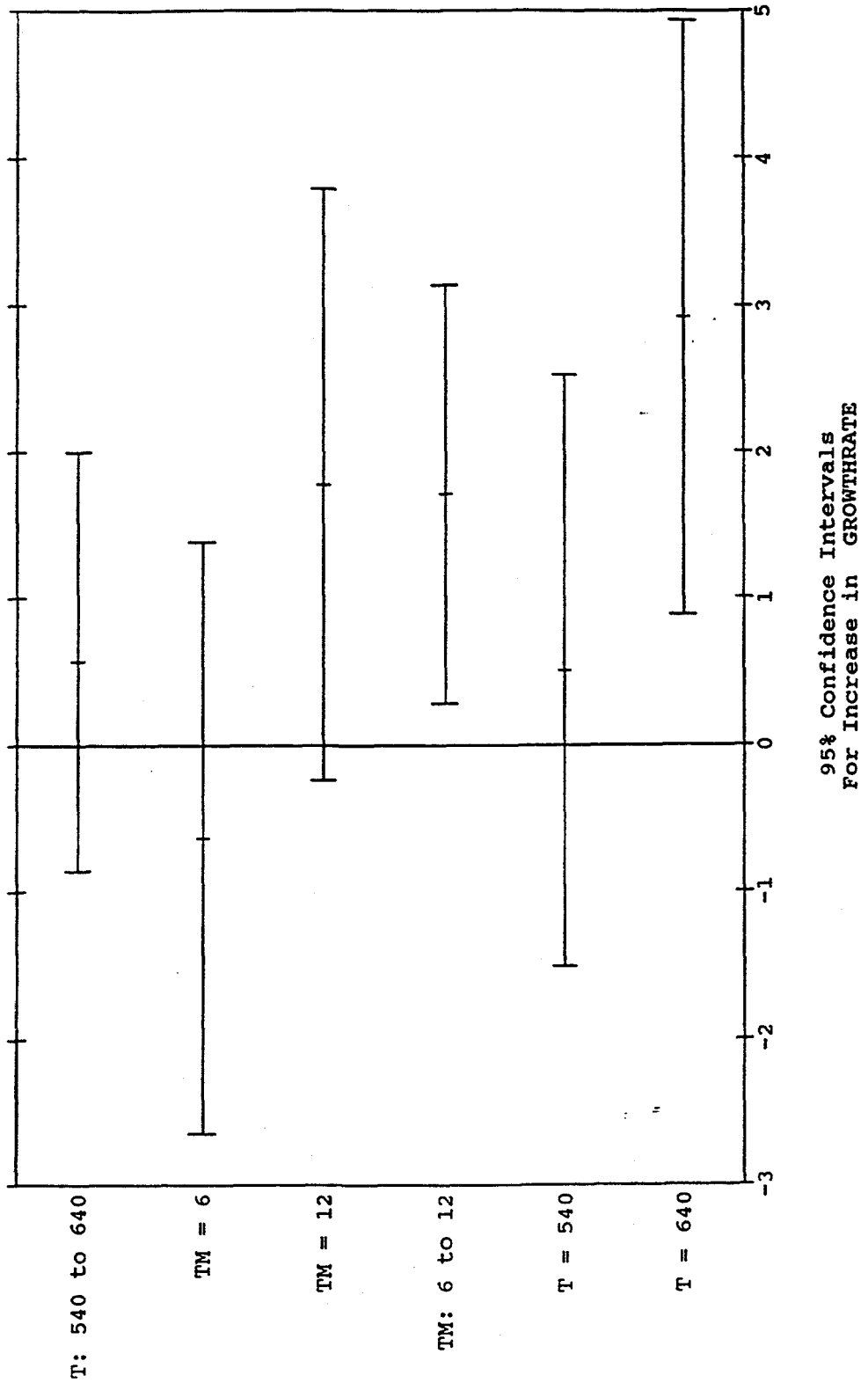


Figure 4.22 Interactive effects of temperature with TMGa flow on response growth rate.

## 4.5 CLEFT Using OM Overgrowth

The screening experiment and analysis provided key insight into the parameter space of interest, but one more function needed to be looked at. This function is the time that it takes to complete the overgrowth of the CLEFT layer. While high overgrowth ratios are desireable, high growth rates are also needed to keep the total growth time down to some reasonable value, particularly for production. Using the RS/1 software and results of the screening experiment, we analyzed the overgrowth time, ie, the inverse of the product of overgrowth ratio and growth rate. The contourplot for the overgrowth ratio and overgrowth time as functions of pressure and HCl flow is shown in Figure 4.23. Surprisingly, the shortest overgrowth times are at the low HCl flows; the growth rate varies more rapidly than the overgrowth ratio. As before, the higher pressure is also desireable.

The overgrowth time data is viewed by HCl flow and TMGa flow in figures 4.24 and 4.25. The shortest times are for low HCl flow and high TMGa flow, with the times decreasing as the reactor pressure is increased. In order to demonstrate the growth rate, we deposited GaAs on CLEFT masks using conditions of 640°C, 130 torr pressure, 12 sccm TMGa flow, 300 HCl flow, and 50 sccm arsine flow. These growth conditions were repeated several times using full 3" GaAs wafers prepared for overgrowth. Continuous films of GaAs were overgrown on three wafers, demonstrating feasibility of this step. The layers were successfully separated from their substrate using the CLEFT process, demonstrating the application of overgrowth using OM chemistry with HCl flow.

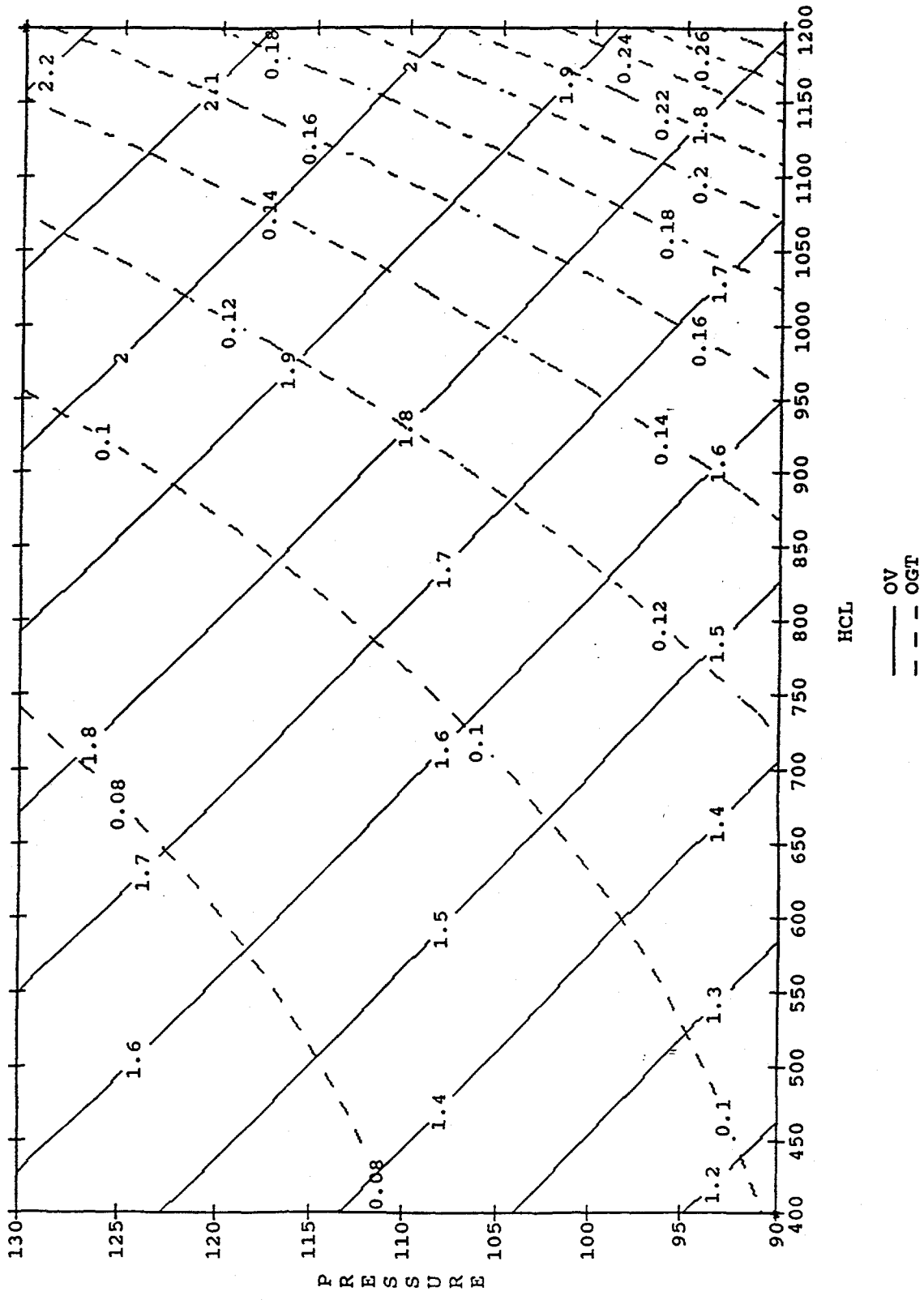


Figure 4.23 Contourplots of overgrowth ratio and overgrowth time as functions of pressure and HCl flow for fixed values of temperature at 640 C, TMGa flow at 12 sccm, and arsine flow of 100 sccm.

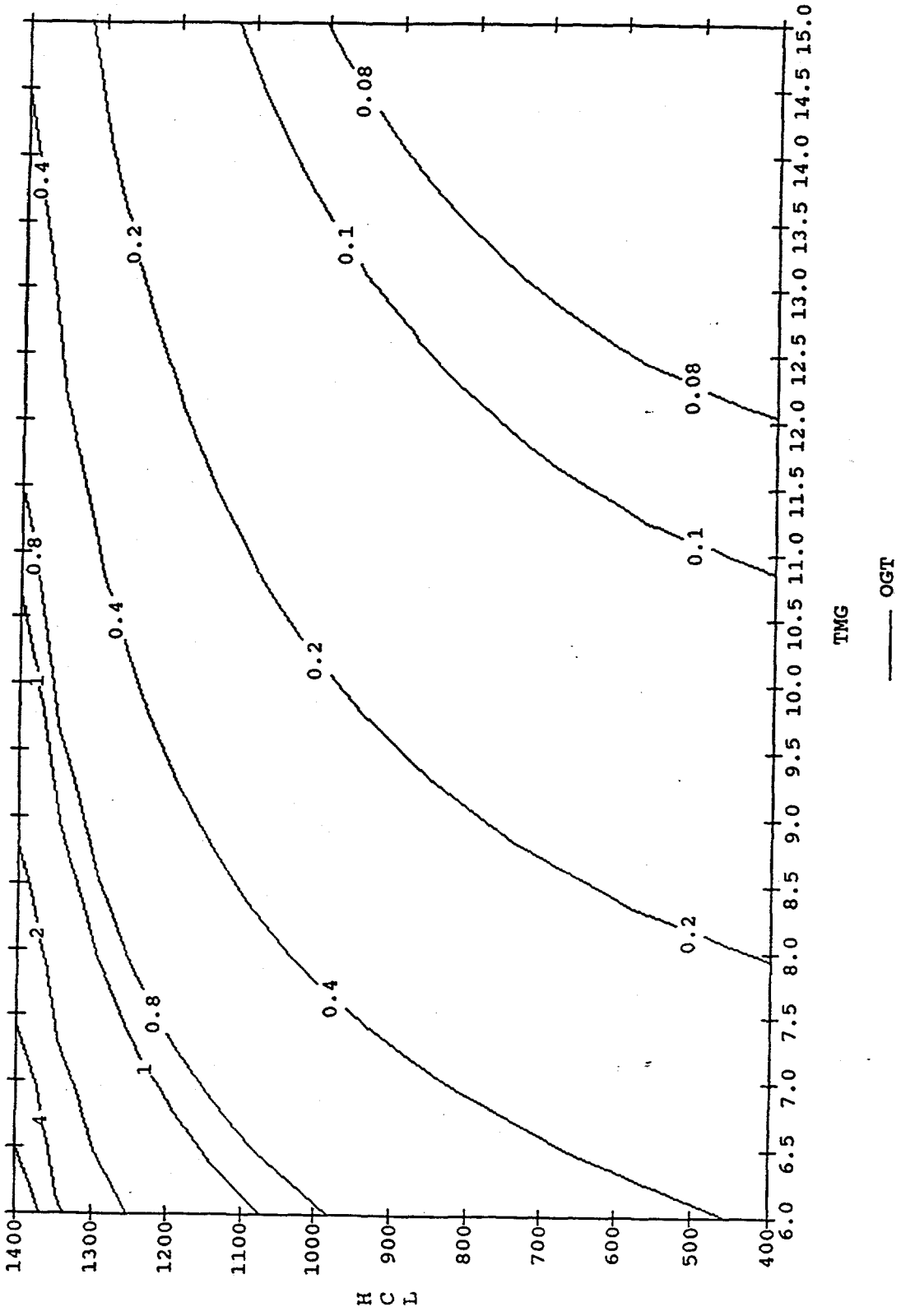


Figure 4.24 Contourplot of overgrowth time as functions of HCl flow and TMGa flow for fixed values of temperature at 640 C, pressure at 110 torr, and arsine flow of 100 sccm.

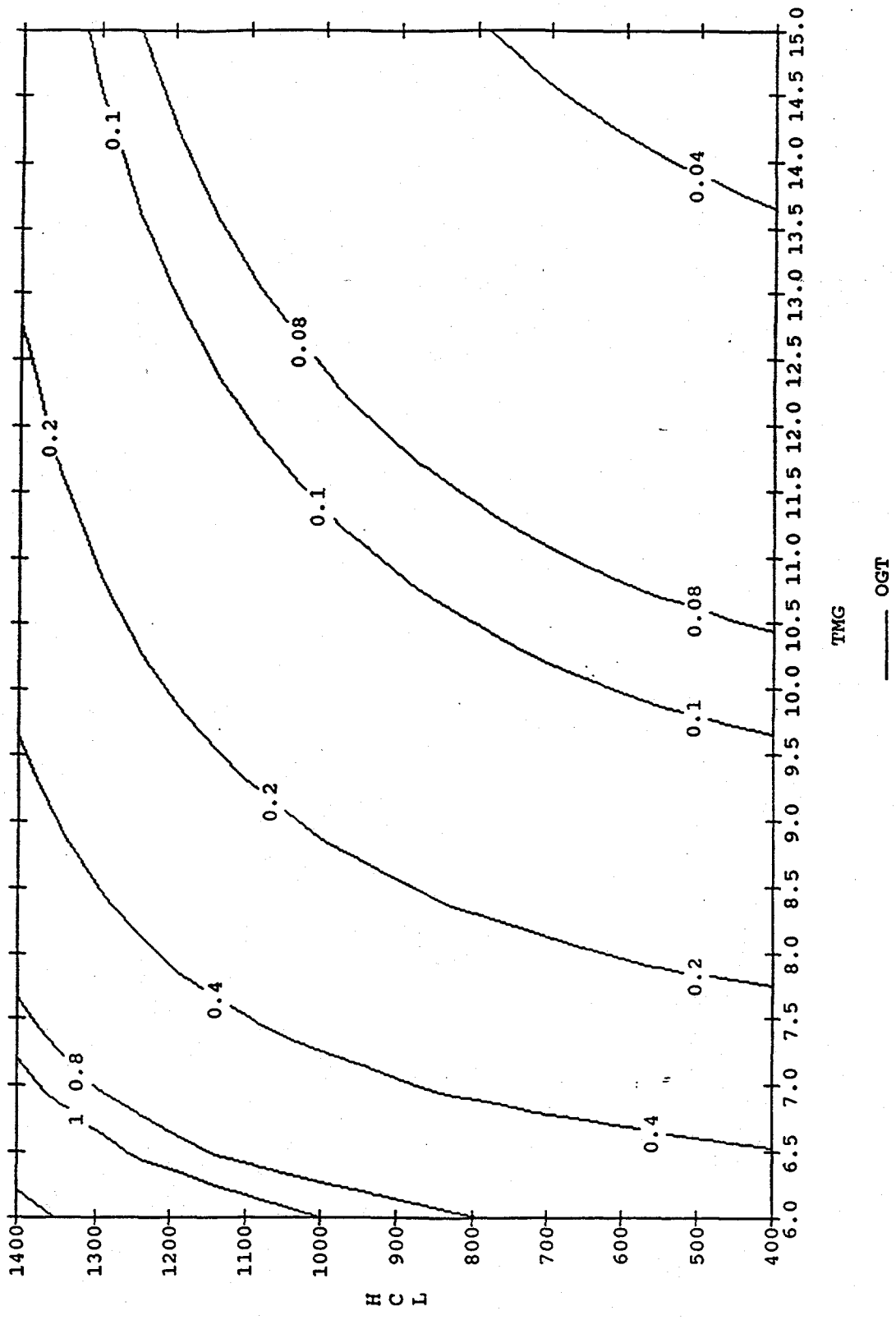


Figure 4.25 Contourplot of overgrowth time as functions of HCl flow and TMGa flow for fixed values of temperature at 640 C, pressure at 150 torr, and arsine flow of 100 sccm.

| Document Control Page | 1. NREL Report No. NREL/TP-451-5746 | 2. NTIS Accession No. DE94000250 | 3. Recipient's Accession No. |
|---|---|---|---|

4. Title and Subtitle
High-Efficiency, Thin-Film Solar Cells

5. Publication Date
January 1994

6.

7. Author(s)
Ronald P. Gale

8. Performing Organization Rept. No.

9. Performing Organization Name and Address
Kopin Corporation
Taunton, Massachusetts

10. Project/Task/Work Unit No.
PV321101

11. Contract (C) or Grant (G) No.
(C) XM-0-19142-4
(G)

12. Sponsoring Organization Name and Address
National Renewable Energy Laboratory
1617 Cole Blvd.
Golden, CO 80401-3393

13. Type of Report & Period Covered
Technical Report
Need Dates Here!!!

14.

15. Supplementary Notes
NREL technical monitor: J. Benner

16. Abstract (Limit: 200 words)

This report describes work on a 3-year research program to investigate thin-film GaAs/GaInP cells using the cleavage of lateral epitaxial film for transfer (CLEFT) technique, and to determine the process to enable overgrowth of GaAs films using organometallic chemistry. The application of the CLEFT thin-film technique to GaInP/GaAs solar cells and organometallic overgrowth was investigated. A problem of alloy contamination was identified and controlled, leading to higher quality layers. Solar cell structures were grown and fabricated using previously determined growth parameters for GaAs and GaInP. With the improved materials developed, significant improvements were made in the performance of the solar cells. Conditions for the in-situ overgrowth by organometallic chemical vapor deposition (OMCVD) were determined and continuous GaAs layers were grown over a separation mask layer. The layers were successfully separated from their substrate using the CLEFT process, demonstrating the application of overgrowth using OM chemistry with HCl.

17. Document Analysis
a. Descriptors
high efficiency ; thin film ; gallium arsendide ; photovoltaics ; solar cells

b. Identifiers/Open-Ended Terms

c. UC Categories
273

18. Availability Statement
National Technical Information Service
U.S. Department of Commerce
5285 Port Royal Road
Springfield, VA 22161

19. No. of Pages
42

20. Price
A03